



POLITECNICO DI TORINO

Department of Electronics and Telecommunications

Master's Degree in Communications and Computer Networks
Engineering

Master's Thesis

**Algorithms for New Radio
synchronization layer functions
(CFO correction, PSS, SSS)**

5G Initial Access

Supervisor

Prof. Roberto Garello

Candidate

Riccardo TUNINATO

matricola: 266701

**Company Supervisors
Telecom Italia**

Eng. Bruno Melis

Eng. Roberto Fantini

ACADEMIC YEAR 2019-2020

Abstract

The 5th Generation technology standard for cellular networks is characterized by the development of a new radio-access technology known as New Radio (NR). It exploits many of the structures and features of 4G Long Term Evolution (LTE), but a rethinking of already consolidated transmission techniques was needed to meet new requirements.

This thesis studies the innovative synchronization methods for 5G.

First of all, the 5G standard defines a new Synchronization Signal Block (SS-Block), i.e. a block consisting of two synchronization signals and one broadcast physical channel. To speed up the initial access process the NR is allowed to use from 8 to 64 synchronization blocks during a variable time interval (not necessarily each radio frame). This leads also to an increasing system complexity. The synchronization procedure at the receiver side is still based on the correlation function but, to maximize performance and to keep low the complexity, an efficient implementation must be found. The starting point consists in the detection of the Primary Synchronization Signal (PSS) and the Secondary Synchronization Signal (SSS). It can be achieved by means of cross correlation of the received signal with local sequence replicas, taken from a predefined set: the real transmitted one is not known a priori. The frequency offset produced by the oscillators non-idealities must be taken into account, since it can disrupt the good correlation properties of the sequences. Choosing when and how to perform its estimation and compensation may strongly affect the performances. Other procedures follow up, using the PBCH (Physical Broadcast CHannel) and the DMRS (Demodulation Reference Signal) inside the SS-Block, to perform channel estimation, to collect Base Station (BS) cell information and more.

It must be considered that NR cells are typically composed by antenna arrays, which are able to perform beamforming and beam sweeping. Thus, the choice of the best beam must be provided, in order to maximize the quality of the transmission.

This thesis is developed by proposal and in collaboration with TELECOM ITALIA. The company is developing a Link Level simulator for 5G, built with Matlab. Its purpose is to model a radio interface which is compliant with 3GPP specification and to evaluate the link level performances of 5G-based point-to-point communications. To this pre-existing tool, the new functions for the synchronization described above must be added. The simulator tries to model the transmission link as accurately as possible, taking into account the characteristics of the wireless channel and the many impairments that can affect the synchronization procedure.

The scope of the thesis is to study and test the techniques for initial synchronization and to evaluate their improvements with respect to LTE. This new algorithms will try to explore the time-frequency characteristics of the m-sequences used inside the SSB.

Contents

List of Tables	III
List of Figures	IV
Abbreviations	VII
Introduction	IX
1 An overview of 5th generation mobile network	1
1.1 The path through the mobile networks standards	1
1.2 Usage scenarios and main goals	3
1.3 Allocation of New Spectrum	6
1.4 Massive MIMO	8
1.5 New Radio (NR)	11
1.5.1 Waveform	11
1.5.2 Multiple access and numerology	13
1.5.3 Duplex Schemes	15
1.5.4 Ultra-Lean Design	16
1.5.5 Backward and forward compatibility	16
1.6 Network slicing	16
2 Initial access and synchronization procedure for an NR receiver	18
2.1 Synchronization in the past mobile networks	18
2.2 The SS-Block	19
2.3 Primary Synchronization Signal (PSS)	22
2.4 Secondary Synchronization Signal (SSS)	24
2.5 Physical Broadcast Channel (PBCH)	25
2.5.1 Demodulation reference signals (DMRS) for PBCH	27
2.6 Providing remaining system information	27
2.7 Random Access	28
3 Description of TIM Physical Layer simulator	30
3.1 Input Parameters	31
3.2 Transmission Chain Modules	32

4	Algorithms and simulation results on Primary Synchronization Signal (PSS) detection	37
4.1	Detection method	37
4.2	PSS detection performance	38
4.3	System parameters	38
4.4	Implementation of Cross Correlation	39
4.4.1	Integer Frequency Offset Estimation	42
4.5	Methodology applied for performance evaluation	45
4.5.1	Threshold tuning	46
4.6	Detector performance in low SINR conditions	46
4.7	Detector performance in CFO estimation	48
4.8	Detector performance in the critical working point	52
4.9	Considering the other PSS sequences	54
5	Physical Broadcast CHannel (PBCH) performance analysis	57
5.1	Frequency Offset effect on the system	57
5.2	Compensation of CFO estimated from PSS detection step	58
5.2.1	Improving frequency offset estimation: time averaging	60
5.3	Timing analysis of the received signal	62
5.3.1	Propagation delay measurements	64
5.4	Complete chain: PBCH processing with both CFO and delay	65
5.5	Simulations with fading channel and beamforming	68
5.6	Extra considerations: a closed loop solution	71
6	Conclusions	74
	Bibliography	76

List of Tables

1.1	Relation between numerology and SCS.	14
2.1	Resources within an SS/PBCH block for PSS, SSS, PBCH, and DM-RS for PBCH [22].	20
4.1	Values of CFO for different possible oscillators' accuracies.	44
4.2	Results from the frequency offset estimation over 20 SSBs.	50

List of Figures

1.1	Time line for forthcoming 5G releases [3].	3
1.2	Usage scenario representation [4].	4
1.3	Performance requirements for high data rate and traffic density scenarios [5].	5
1.4	Atmospheric attenuation versus frequency [17].	7
1.5	Example of the radiation pattern of an antenna array.	9
1.6	Example of the frequency domain orthogonality of sinc-squared per-subcarrier spectrum.	12
1.7	LTE OFDMA Time/Frequency resource allocation.	14
1.8	Simple representation of FDD and TDD schemes.	15
2.1	SS/PBCH block structure [28].	20
2.2	Multiple time-multiplexed SS blocks within an SS-burst-set period [20].	22
2.3	PSS time and frequency offset ambiguity of (a) LTE PSS sequence (left) and (b) NR PSS sequence (right) [21].	23
2.4	Radioframe synchronization procedure [23].	27
2.5	5G NR synchronization procedure [19].	29
3.1	5G Physical Downlink Shared Channel (PDSCH) Transmission chain. .	31
3.2	representation of the direction of the antennas w.r.t. the RX device. . .	33
3.3	A block-scheme representation of an OFDM modulator.	34
4.1	Subframe organization.	39
4.2	Example of FIR matched filter.	40
4.3	Quality indicator in case when no channels or signals are transmitted, except for PSS.	41
4.4	Quality indicator in case when all channels and signals are transmitted, using Kaiser filtering, w.r.t. an ideal case.	42
4.5	Quality indicator in case when no channels or signals are transmitted, except for PSS, using also Kaiser filtering.	42
4.6	Simulator block scheme with PSS detection.	43
4.7	PSS detector functions.	44
4.8	Example of the PSS detector output with the threshold comparison. . .	47
4.9	PSS detection performance with SINR = -6 dB.	48
4.10	PSS detection performance with SINR = -8 dB.	48
4.11	PSS detection performance with SINR = -10 dB.	49
4.12	PSS detection performance with SINR = -12 dB.	49

4.13	PSS detection performance with $FO = 0$ Hz.	50
4.14	Frequency Offset measurements: mean value for different SINR levels. .	51
4.15	Frequency Offset measurements: standard deviation for different SINR levels.	51
4.16	Frequency Offset measurements: root means square error for different SINR levels.	52
4.17	Critical working point: Behaviour of probability of correct detection w.r.t CFO.	53
4.18	Critical working point: CFO estimated mean and standard deviation. .	53
4.19	PSS m-sequence cross-correlation, among the three possible different PSSs when PSS_0 is transmitted.	55
4.20	Hardware implementation for the PSS detection, considering three possible sequences.	56
4.21	Bars counting if and which PSS sequence has been detected, in case of different SINRs and CFOs, when PSS_1 is transmitted.	56
5.1	BLER for PBCH whit CFO insertion, 1 RX antenna.	58
5.2	BLER for PBCH whit CFO insertion, 2 RX antennas.	59
5.3	BLER for PBCH whit CFO insertion, 4 RX antennas.	59
5.4	Comperison of BLER for PBCH for different number of RX antennas (no CFO).	60
5.5	BLER for PBCH whit CFO insertion and compensation, 1 RX antenna. .	61
5.6	BLER for PBCH whit CFO insertion and compensation, 2 RX antennas. .	61
5.7	BLER for PBCH whit CFO insertion and compensation, 4 RX antennas. .	62
5.8	BLER for PBCH whit CFO insertion and compensation with time accumulation, 1 RX antenna.	62
5.9	BLER for PBCH whit CFO insertion and compensation with time accumulation, 2 RX antennas.	63
5.10	BLER for PBCH whit CFO insertion and compensation with time accumulation, 4 RX antennas.	63
5.11	PBCH processing results w.r.t. delay, @ 100 dB SINR.	65
5.12	PBCH processing results w.r.t. delay overcompensation, @ 100 dB SINR. .	65
5.13	Comparison with the two timing cases, @ 100 dB SINR.	66
5.14	Scattering diagrams @ 100 dB SINR, $D_1 = 144$ samples (1/2 CP) . . .	66
5.15	Scattering diagrams @ 100 dB SINR, $D_2 = 288$ samples (as CP length). .	67
5.16	Scattering diagrams @ 100 dB SINR, $D_3 = 360$ samples (as CP length). .	67
5.17	PBCH BLER behaviour with both delay and CFO (of 1.8 kHz) addition. .	68
5.18	PBCH BLER behaviour with both delay and CFO (of 3.6 kHz) addition. .	68
5.19	PBCH BLER behaviour for a 32x4 configuration with beamforming, fading channel and both delay (1/4 CP) and CFO (of 3.6 kHz) addition. .	70
5.20	PBCH RAW BER behaviour for a 32x4 configuration with beamforming, fading channel and both delay (1/4 CP) and CFO (of 3.6 kHz) addition. .	70
5.21	A block scheme example of RX with frequency acquisition and tracking. .	71
5.22	PSS detection module	72
5.23	CFO estimates distribution.	73

Abbreviations

3GPP	3rd Generation Partnership Project
BS	Base Station
CFO	Carrier Frequency Offset
CP	Cyclic Prefix
DMRS	Demodulation Reference Signal
FDD	Frequency Division Duplexing
ICI	Inter Carrier Interference
ISI	Inter Symbol Interference
LTE	Long Term Evolution
MIMO	Multiple Input Multiple Output
NR	New Radio
OFDM	Orthogonal Frequency Division Multiplexing
PBCH	Physical Broadcast Channel
PSS	Primary Synchronization Signal
RB	Resource Block
SCS	Subcarrier Spacing
SINR	Signal to Interference plus Noise Ratio
SSS	Secondary Synchronization Signal
SSB	Synchronization Signal Block
TDD	Time Division Duplexing
TTI	Time Transmission Interval
UE	User Equipment

Acknowledgements

I thank my company supervisors from Telecom Italia, Roberto Fantini and Bruno Melis, with whom I have had the pleasure of collaborating in these months, for the trust and support they have never made me lack.

I also thank Roberto Quasso, who was often present and helpful during our weekly calls, and Marco Caretti, for supporting the collaboration.

I thank my supervisor, prof. Roberto Garelo, who allowed me to start this project, and to accomplish it thanks to his wise advice and his unconditional availability.

I thank my parents Alessandro and Costanza, to whom I could never have asked for more than everything they have already done for me.

I thank my sister Alice and her partner Enrico, for being a reliable and positive presence in my life.

I also thank all the colleagues and friends that I have had the pleasure of meeting these years, who have made all the steps of my life path more enjoyable.

Introduction

In 2020, the 5th generation standard for cellular networks is no more an idea belonging to the future, but a well-known technology whose implementation has already begun. It has not to be meant as a standalone system that comes at a certain time, and that will be then simply replaced in few years by the next generation. The mobile network technologies instead are continuously growing, without being limited by the particular version of the standard. Researchers are progressively pushing further the current techniques and algorithms, acting like a machine that never sleep, trying to exploit the available resources as much as possible. This is the context where this thesis finds its place.

Among the many wireless communication topics touched by 5G, one of the most studied in the past is the synchronization and initial access procedure at the physical layer, yet it is still fundamental in the innovation process today. The first operation for initial access is cell searching, the first step before the actual data exchange. It is almost transparent to the users but it plays a key role in attempting to meet the new requirements, driven by the need for low latency, energy efficiency and flexibility. The use of new bands at higher frequencies is characterized by greater impairments on signal propagation through the channel, so the advancement must be aimed at recovering from this undesired aspect.

It follows a rethinking of the communication rules between the Base Station (BS) and User Equipment (UE) in 5G New Radio (NR). In particular, a more flexible technology is envisaged depending on the available resources, the environment and the required performance. Giving the system the possibility to adapt to different situations is a huge jump towards a smarter technology, but it comes with a price. We must consider a wider range of scenarios, and so develop new algorithms able to work smoothly trying to keep low the overall complexity. The already available solutions are often outdated, and a deep study to find the right new choices must be performed.

Different techniques are available in the literature, but not many results have been collected on their implementation. Moreover, often the bigger pictures of all the transmission chain is not investigated, focusing only on some limited aspects. Our aim is then to study the synchronization procedure in a more complete way, providing a detailed system simulating as good as possible the real world. Moreover, algorithms must take into account the actual available devices and so a further implementation in hardware, through Field Programmable Gate Arrays (FPGA).

This document is organized as follows:

First chapter Overview of the main interesting points of 5G. A quick roadmap goes through the past mobile standards technology up to the current one. The scenarios of interest that motivate the need of innovations in the mobile networks are presented, with their requirements. The principal solutions that will make it possible to achieve the new demands are listed, with a deeper description of the 5G NR.

Second chapter Precise explanation of the synchronization procedure in the initial access, which is the main topic of this thesis. In particular, the discussion is focused on the characteristic of the Synchronization Signal Block (SSB) transmitted by the network antenna system, and on how the devices can use it for cell searching and system information recovery. There is also a short description of the following Random Access procedure, used to actually establish the connection between the device and the network.

Third chapter Introduction of the Matlab simulator developed and provided by TIM, which tries to model the transmission chain from the generation of the channels and signals by the transmitter to their recovery at the receiver. Algorithms from which the results are obtained are developed on top of this already existing simulator, extending its capabilities.

Fourth chapter Presentation of software solutions and their results on the Primary Synchronization Signal (PSS) detection. The cross correlation function is employed, through a matched filter preceded by an Anti Aliasing filter, which correct design is fundamental to obtain an acceptable behaviour. A quite large variety of situations have been considered, with a particular underline on Carrier Frequency Offset (CFO) estimation and compensation behaviour.

Fifth chapter Analysis focused on another key step of synchronization, the decoding of the Physical Broadcast Channel (PBCH). The generation and demodulation of this physical channel is available in the simulator, but deeper studies on the process behaviour are required. In particular, it must also be taken into account the correction on system time/frequency impairments, thanks to the previous PSS detection. Different configurations of Multiple Input Multiple Output (MIMO) antenna systems are considered, allowing different type of techniques to improve the estimation accuracy.

Chapter 1

An overview of 5th generation mobile network

1.1 The path through the mobile networks standards

Many technologies and systems emerged from the world of communications networks, that profoundly changed our way of life, both from a social and economic point of view. There is a variety of applications and devices we are using today no one would ever believe the existence just few decades ago, and mobile broadband networks are of course part of it.

Before arriving at current systems, their development followed a long path, which can now be referred to as the history of mobile networks ([2], [1]):

1G, ~ 1980 First generation of mobile network, 1G, was still based on analogue transmission, and only voice was the targeted service. Other wireless radio communications technologies already existed before 1G, but the turning point was the relatively large pool of servable users, opening much further the system to the public. Different 1G solutions have been developed, even if the fundamental characteristics were similar, as for the Frequency Division Multiple Access (FDMA). The two principal were Total Access Communication System (TACS), mainly in Europe, and Advanced Mobile Phone Service (AMPS), in the US.

2G, ~ 1990 After a decade, the Second Generation (2G) made the transition of mobile networks to the digital domain, motivated by several advantages: new coding techniques became available, to support integration of different services, like Short Message Service (SMS), cryptography and advanced voice coding to reduce bandwidth. Since no internationally recognised entity existed to guide this innovation process, many second generation technologies came up: in Europe and in Japan,

with Global System for Mobile Communications (GSM) and Personal Digital Cellular (PDC) respectively, both based on FDMA/TDMA, and in the US, with IS-95 using Code Division Multiple Access (CDMA). Main goals were the use of new frequency bands (850, 900, 1800, 1900 MHz), smaller cells and better efficiency. The first solution providing feasible data services is 2.5G (GPRS/EDGE in Europe, IS-95B in USA), an evolution of 2G that granted higher speed and packet-switching forwarding.

3G, ~ 2000 As the Internet was gaining the world interest, a new standard became necessary, leading the transition from voice-centric systems to data-centric systems. At the same time, the need of a global standardization grew, in order to cut costs and offer a common standard for a large number of manufacturers and users. 3rd Generation Partnership Project (3GPP) was then established, leading the definition of 3G, mainly composed by European and Japan entities, joined by the use of wideband CDMA (WCDMA) technology (UMTS). In the US a different system was employed, the CDMA2000 (IS-95C). Higher data rates (up to 2 Mbps) and overall improved performance were achievable thanks to smaller cells with high capacity and larger cells to support mobility of fast users.

An effectively large improvement in the data rates came up with HSPA, an evolution of UMTS, with data rates up to 56 Mbps in download.

4G, ~ 2010 3GPP was so successful that, despite its name, kept on working for the successive standard, the 4G. 4G is usually know as Long Term Evolution (LTE), while another 4G technology, WiMax, had not the same spread and success. One of the main targets of LTE were an improvement of performance in terms of capacity, to sustain the new data greedy applications (such as video streaming), and support for scenarios that are difficult to communicate, such as in the case of users on the move.

A decade is roughly the time passed between the introduction of each new standard, and the same goes for the transition from 4G to the new 5th Generation technology standard for cellular networks, 5G. Partial versions of 5G have already been installed, referred as non stand-alone systems, but the full specifications are not yet met.

It is important to note that each generation is not completely independent from the previous: the standards are mostly a definition of the requirements the system should comply with, but the technologies are actually continuously evolving and adding new features, despite being called with the same name. For example, HSDPA had higher data rates with respect to UMTS, both technologies within 3G. To classify the various phases of mobile networks evolution, with greater temporal resolution, different releases are defined for each generation. For 5G, the first version is contained in release 15, which is a middle ground between 4G and 5G, since not all the new requirements can be satisfied. In figure 1.1 is shown a time line of the forthcoming 5G releases.

5G is characterized by a new radio-access technology, but its importance lies in the use of new solutions on different levels: "5G is also often used in a much wider context,

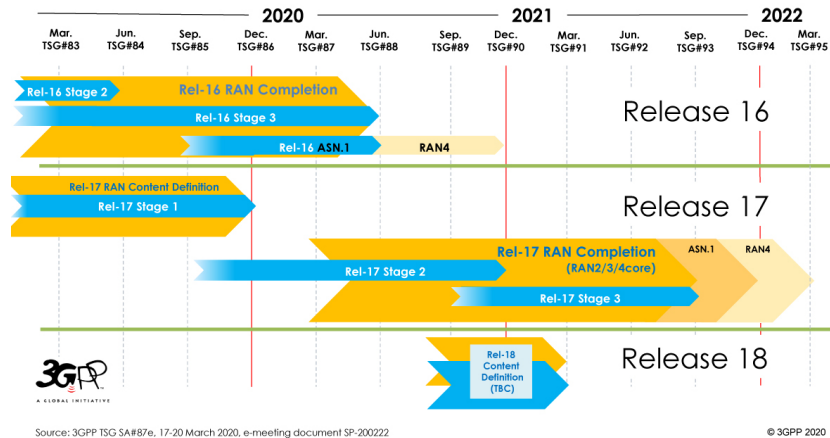


Figure 1.1: Time line for forthcoming 5G releases [3].

not just referring to a specific radio-access technology but rather to a wide range of new services envisioned to be enabled by future mobile communication" [1].

1.2 Usage scenarios and main goals

The upcoming 5th Generation mobile network technology is the foundation of the digital transformation the society is trying to achieve these years. It is difficult today to think about new business activities that would not benefit from an advanced digital and connected environment. However, the needs of each user can be very different, and this is the problem 5G is aiming to solve: supply a flexible system able to satisfy a large variety of situations.

Three main classes of usage scenario have been defined:

1. **enhanced Mobile BroadBand (eMBB)**. It corresponds to the more traditional improvement of the mobile broadband services, aiming to keep up with the continuously growing demand of high data rates, caused by services that require the transmission of a large amount of data with few delays, such as Ultra-High Definition (UHD) video, virtual reality (VR), and augmented reality (AR). "Global mobile data traffic will increase nearly eightfold between 2015 and 2020. Mobile data traffic will grow at a compound annual growth rate (CAGR) of 53 percent from 2015 to 2020, reaching 30.6 exabytes per month by 2020" [6].
2. **massive Machine-Type Communication (mMTC)**. It consists of a network where a massive number of devices communicates. They are called machines since they do not need a physical interface with the user, like remote sensors. The main challenge is to attach a large number of low-rate low-power devices, as large as billions of interconnected devices within the paradigm of the Internet of Things (IoT): low-rate because only small amount of data is exchanged, and low-power

since they are powered by batteries which should last several years, also considering the common difficulties on substitution interventions. Another characteristic is that the transmissions can be sporadic and asynchronous. Thus there will be an unknown, random subset of devices being active at a given transmission instant or frame, which necessitates the use of some form of random access protocol[7].

3. **Ultra-Reliable and Low-Latency Communication (URLLC)**. It is related to new expectations of very low latency and extremely high reliability, for example for Industry 4.0. This name refers to the new industrial revolution based on the automation and data exchange in manufacturing technologies, which benefits from ICT advances of Internet and communication revolution [8]. To obtain an efficient automation process an almost real-time operability is mandatory, with the least possible error rate. Other examples can be found in traffic safety, such as assisted and automated driving, a very latency-sensitive service.

Not all the possible scenarios reside in these three definitions, and the requirements can overlap among them. Figure 1.2 tries to represent the wide range of possible applications.

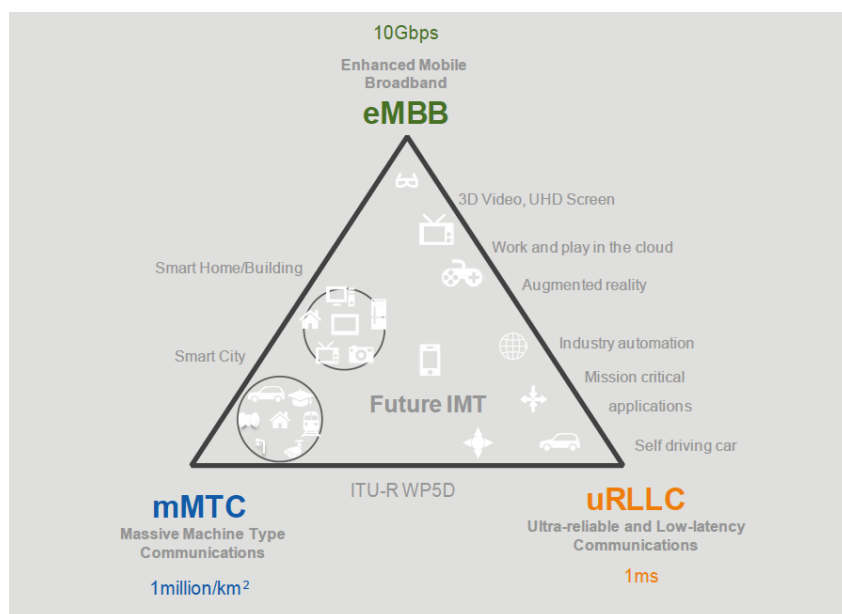


Figure 1.2: Usage scenario representation [4].

Another step in the standard design is the definition of Key Performance Indicator (KPI), i.e. particular requirements linked to each usage scenarios, which developer must satisfy when providing a new system, as resilience and strong surge of emergency communications during natural disaster and ultra-high availability and reliability for public safety.

The key word is thus flexibility, and 5G should be considered not a specific radio-access technology but rather defined by the use cases to be supported [2]. The definition

of the general performance that we expect from 5G is not straightforward, since it has to take into account the type of traffic, the usage scenario, the characteristics of the environment and more. Quite complete specifications can be found in figure 1.3, where it is however possible to notice the considerable capabilities that the new mobile networks could achieve.

	Scenario	Experienced data rate (DL)	Experienced data rate (UL)	Area traffic capacity (DL)	Area traffic capacity (UL)	Overall user density	Activity factor	UE speed	Coverage
1	Urban macro	50 Mbps	25 Mbps	100 Gbps/km ² (note 4)	50 Gbps/km ² (note 4)	10 000/km ²	20%	Pedestrians and users in vehicles (up to 120 km/h)	Full network (note 1)
2	Rural macro	50 Mbps	25 Mbps	1 Gbps/km ² (note 4)	500 Mbps/km ² (note 4)	100/km ²	20%	Pedestrians and users in vehicles (up to 120 km/h)	Full network (note 1)
3	Indoor hotspot	1 Gbps	500 Mbps	15 Tbps/km ²	2 Tbps/km ²	250 000/km ²	note 2	Pedestrians	Office and residential (note 2) (note 3)
4	Broadband access in a crowd	25 Mbps	50 Mbps	[3,75] Tbps/km ²	[7,5] Tbps/km ²	[500 000]km ²	30%	Pedestrians	Confined area
5	Dense urban	300 Mbps	50 Mbps	750 Gbps/km ² (note 4)	125 Gbps/km ² (note 4)	25 000/km ²	10%	Pedestrians and users in vehicles (up to 60 km/h)	Downtown (note 1)
6	Broadcast-like services	Maximum 200 Mbps (per TV channel)	N/A or modest (e.g., 500 kbps per user)	N/A	N/A	[15] TV channels of [20 Mbps] on one carrier	N/A	Stationary users, pedestrians and users in vehicles (up to 500 km/h)	Full network (note 1)
7	High-speed train	50 Mbps	25 Mbps	15 Gbps/train	7,5 Gbps/train	1 000/train	30%	Users in trains (up to 500 km/h)	Along railways (note 1)
8	High-speed vehicle	50 Mbps	25 Mbps	[100] Gbps/km ²	[50] Gbps/km ²	4 000/km ²	50%	Users in vehicles (up to 250 km/h)	Along roads (note 1)
9	Airplanes connectivity	15 Mbps	7,5 Mbps	1,2 Gbps/plane	600 Mbps/plane	400/plane	20%	Users in airplanes (up to 1 000 km/h)	(note 1)

NOTE 1: For users in vehicles, the UE can be connected to the network directly, or via an on-board moving base station.
 NOTE 2: A certain traffic mix is assumed; only some users use services that require the highest data rates [2].
 NOTE 3: For interactive audio and video services, for example, virtual meetings, the required two-way end-to-end latency (UL and DL) is 2-4 ms while the corresponding experienced data rate needs to be up to 8K 3D video [300 Mbps] in uplink and downlink.
 NOTE 4: These values are derived based on overall user density. Detailed information can be found in [10].
 NOTE 5: All the values in this table are targeted values and not strict requirements.

Figure 1.3: Performance requirements for high data rate and traffic density scenarios [5].

In order to satisfy the described targets, new key technological enablers have been designed. They do not belong only to network and communication fields, but they spread to new concepts coming from other fields.

A presentation of the main novelties is reported in the next sections, with particular interest for those concerning the physical level, given their study for the effective development of the thesis work.

1.3 Allocation of New Spectrum

Throughput of a communication system is one of the main performance indicator. Its theoretical upper bound can be computed thanks to the Shannon theorem, as follows:

$$C_{max} = B \cdot \log_2\left(1 + \frac{P_{RX}}{P_N}\right) \quad (1.1)$$

Where C is the capacity, B is the bandwidth and $\frac{P_{RX}}{P_N}$ the ratio of the useful signal received power over the noise power. In this relation the capacity of the system increases linearly with the bandwidth, one of the most valuable resources when deploying a wireless network. At the same time its deficiency could become a huge limitation, since alternatively only P_{RX} can be improved (at least in this formula), but with a logarithmic relationship.

4G has reused the bands from previous standards and added new ones, which collectively are located in a frequency range from 450 MHz to around 6 GHz. 5G will continue to work with these bands, but not many others are available within these boundaries. Other wireless mobile network systems occupy these frequencies, and now there is overcrowding in the spectrum up to a few GHz.

To find new and plenty free bandwidth 3GPP had to exploit further the *medium-frequency bands* in the range of 3-6 GHz, and had to look at higher frequencies, in the so called mm-Wave range, corresponding to the High-frequency bands above 24 GHz. "The highest interest is in the range 24.25-29.5 GHz, with 3GPP NR bands n257 and n258 assigned. Channel bandwidths up to 400 MHz are defined for these bands, with even higher bandwidths possible through carrier aggregation"[9].

The range of frequencies adopted by a certain system can deeply influence the signal propagation characteristic, so a distinction in two frequency ranges becomes useful in the analysis and design phase:

Frequency range designation	Corresponding frequency range
FR1	450 MHz – 6000 MHz
FR2	24250 MHz – 52600 MHz

Considering that 5G system will maybe be able to exploit also bands above 60 GHz, it will be possible to revise these designations. While FR1 comprehends most of the already used bands, FR2 will be exclusively related to new 5G bands, and will require the installation of completely new systems.

As mentioned before, channels with very large bandwidth are available at higher frequencies, but the reception of the transmitted signal is subject to greater challenges, since *path loss*¹ increases with frequency. This behaviour is described by the Friis equation, which gives the power at the receiver (P_{RX}), in a free space link in Line Of Sight

¹Attenuation of the signal during its propagation

(LOS), considering the attenuation of the signal:

$$P_{RX} = \frac{G_{TX}G_{RX}P_{TX}\lambda^2}{(4\pi d)^2} \quad (1.2)$$

where P_{TX} is the transmitted power, G the antenna gains (equal to 1 in case of isotropic antenna), d the distance between TX and RX, and $\lambda = \frac{c}{f}$ the wavelength. It is clear how P_{RX} decreases quadratically as the frequency (and distance).

Moreover, at lower wavelengths, the signal suffers more of blockage. Smaller obstacles increases the attenuation, such as leaves of trees (foliage loss) or rain. Atmospheric losses are then critical issues to be taken into account, and their attenuation curves presents some peaks for certain frequencies (figure 1.4). These frequencies should be used where influence of atmospheric attenuation is not significant, e.g., for small cells and for indoor usage [17].

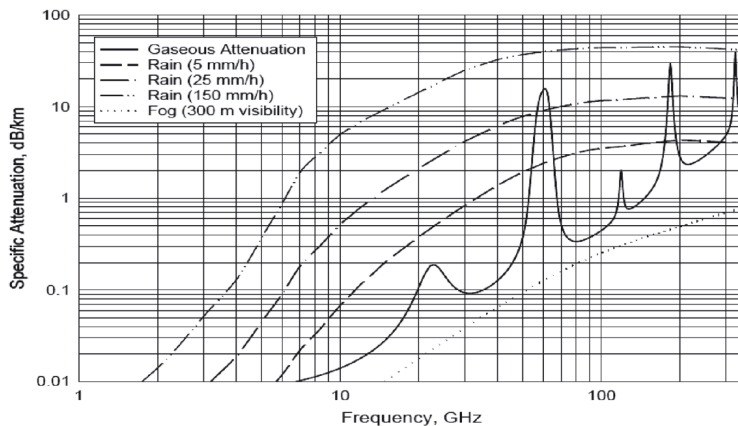


Figure 1.4: Atmospheric attenuation versus frequency [17].

From these considerations it follows that these bands can only be used for transmissions in cells with limited coverage, but providing large bandwidths to satisfy high data rates and numerous users.

Thinking about common antenna systems, the idea of installing new big towers with such limited coverage seems a not so great deal. Fortunately, the size of the antennas is proportional to the wavelength of the signal, so the new BSs could be installed also in pre-existing buildings and structures, like light street lamps. Another advantage is that antenna arrays can be exploited. They are collection of antennas that combines each output/input to enhance the total received/transmitted signal. Antenna arrays enable new solutions, like the management of the radiation pattern without a mechanism that physically moves the antenna. This beam steering can be realized by simply modifying the relative phase shifts and amplitudes of the array elements [10], the basic principle of beamforming (more in the next section of MIMO). This solution will alleviate the strong channel *path loss*.

The 5G architecture will therefore provide an ultra-dense scenario composed of a multitude of small and micro cells, based on high frequency band, supported by the more conventional macro cells at medium and low frequencies, to ensure complete coverage and maximum performance, also avoiding the link blockage due to even small obstacles. These elements will have to cooperate together efficiently, avoiding interference and taking advantage of the properties of both frequency ranges.

1.4 Massive MIMO

Multiple Input Multiple Output (MIMO) is referred to systems which exploit more antennas at both transmitter and receiver side (like antenna arrays). MIMO systems are being the focus of interest in many studies, in order to respond to the increasing rate demand of wireless networks.

More than one antennas at the transmitter (TX) and/or receiver (RX) can be used for different kind of solutions:

1. **Diversity:** For long time before the MIMO-concept advent, the presence of multiple antennas has been exploited at the RX side, by mean of the receiver Diversity. The basic idea is the usage of 2 or more antennas at RX side to improve the signal quality, even if only one TX antenna is used (Single Input Multiple Output, SIMO). With a proper spacing between antennas ($\geq 0.5 \cdot \lambda$) and if antenna gains are uncorrelated, each antenna receives the same transmitted signal, but with a different frequency response. Thus, low signal strength measured by one antenna, could not be a problem for the data exchange, since at another antenna the signal strength could be high enough to guarantee a sufficiently low error rate (there is a compensation among them). The probability of Deep Fade, i.e. a Signal to Interference plus Noise Ratio (SINR) so weak that the symbol can't be correctly recovered, is so greatly reduced. The simplest Diversity technique is the Selective Combination, by choosing the symbol with the maximum power among all the versions of the different antennas. A more efficient technique is the Maximum Ratio Approach, which combines all the different versions of the received symbols, but requires an accurate channel estimation. A completely dual approach is diversity at TX side, by transmitting the same signal through more antennas (Multiple Input Single Output (MISO)). The non correlation of antenna gains is a fundamental condition, and it is achievable in rich scattering environments, where multipath produces many reflections, so each antennas "sees" an independent spatial channel.
2. **Directivity (Beamforming or spatial filtering):** Directivity is a signal processing technique used with antenna arrays for directional signal transmission or reception. The change of directionality in the antenna array is realized by controlling the relative phase and amplitude of the signals at each antenna element. MIMO systems requires a precoding block to transform a vector of QAM symbols to be transmitted into a vector of L complex symbols, which are actually

transmitted over the channel, by using L antennas. Beamforming is a simplified form of precoding where a symbol is multiplied by a beamforming vector b , and usually the elements of b are simple phase shifts. The radiation pattern is then characterized by a main beam and minor secondary lobes, thus concentrating the signal power only along a certain direction (an example in figure 1.5). The gain of the antenna is increased, and thus the capacity and coverage of the Base Station (see Equation 1.2), unlike the common isotropic antennas with a gain of 0 dB in each direction.

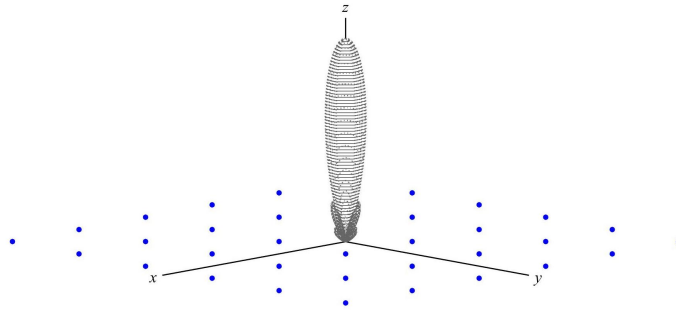


Figure 1.5: Example of the radiation pattern of an antenna array.

The maximum gain depends on the number of array elements, since constructive and destructive interference is exploited.

3. **Spatial Multiplexing:** Just like Frequency multiplexing and Time Multiplexing, the different paths the signal go through, before reaching the RX antennas, can be exploited to carry different data streams. The condition, as for diversity, is the existence of independent channels, and a good knowledge of the channel matrix at the transmitter and at the receiver side, to correctly define a precoding matrix, used to transform a single data stream into a set of different streams. Its importance is represented by the capability to redefine the limit of Shannon's capacity:

$$C_{total} = C_1 + C_2 + \dots + C_L = L \cdot B \cdot \log_2\left(1 + \frac{P_{RX}}{P_N}\right)$$

L , the number of exploitable different streams, is upper limited by the minimum between the number of the antenna elements of transmitter and receiver: $L \leq \min(N_{TX}, N_{RX})$. At first glance, it could be said that C_{total} grows linearly with the number of L spatial channels. To be precise, this result is correct only considering that the total TX-ed power is kept constant for each antenna, and

not divided among them.

Spatial Multiplexing can be used also to transmit the same data flow in different spatial channels, taking advantage of this new kind of redundancy to increase the robustness against errors. Special codes as Linear Space-time block codes (LST-BCs) have then been designed, mapping a set of symbols to a matrix suitable for the MIMO configuration.

The MIMO concepts is already present in LTE and LTE-Advanced radio interfaces, mostly for spatial multiplexing, with configuration up to 8x8 MIMO (8 transmitting and 8 receiving antennas), allowing to reach peak data-rates as high as 3 GBps (over 100 MHz with Carrier Aggregation). Another option for MIMO system is based on allocation of the streams among users: if all the streams are reserved for only one user then it is a Single User MIMO (SU-MIMO), otherwise it is a Multi Users MIMO (MU-MIMO). The last releases allow for a dynamic switching between these modalities. In 5G, MIMO retains a central role and its functionalities are extended in the so-called Massive-MIMO. This name comes from the possible increase of the number of antennas with respect to current MIMO systems by an order of magnitude (i.e. from several tens to hundred antennas). The implemented solution is different depending on the frequency range operation: at lower frequencies, more users are served in parallel on the same time-frequency resources (MU-MIMO), while at higher frequencies greater beamforming gains can be achieved, counteracting path loss.

New antenna systems are introduced to support the possible MIMO configurations, as the 2D Active Antenna System (AAS). It can be composed by a large number of antennas placed in a 2D plane, keeping a relatively low space occupation with respect to linear array that could reach too high lengths.

When beamforming is employed, the devices initial access could become quite tricky, since at the beginning no information is available on the beam disposal and time availability. Beam-related functions are then critical aspects of communication reliability, included in the beam management set of procedures needed to acquire and maintain a set of TRxP (Transmitting/Receiving Points for each cell) and/or UE beams that can be used for DL and UL transmission/reception:

Beam sweeping technique developed by BS to transmit control and synchronization information over the entire cell, alternating the transmission between all possible directions, with their relative beams, that can then be very narrow (and so with very high gain).

Beam measurements through the reference signals inside a certain beam, the UE can estimate its relative channel goodness.

Beam selection depending on the measured quality of the signals from the different beams, the UE chooses the most suitable one, which should correspond to the one steering at the device.

Beam reporting for UEs to report information of beamformed signals based on beam measurement.

Another characteristic of beamforming is that it can be implemented in analog or digital domain, or even in an hybrid way, largely influencing the flexibility and complexity of the system. Digital beamforming permits a dynamic software definition of the precoding matrix, so adapting the actual radiation pattern also to temporary needs and devices presence in the cell. A dynamic adaptation to unpredictable interference can be managed by ad-hoc algorithms, particularly relevant in the 5G ultra-dense scenario. An example of phase-only synthesis of antenna arrays in the presence of Gaussian interference is addressed in [14]. The drawback is the need of a modulation chain for each antenna, resulting in a significantly high complexity and power consumption. Analog beamforming, on the other hand, makes available a very light system, where phase shifts are simple delay lines after the digital-to-analog conversion. The complexity is then kept very low, but not much flexibility is available. This is the actual feasible solution for high frequencies systems, where signal processing already reaches rates limit. An hybrid solution can be employed, balancing the previous two. A goal of the massive MIMO for 5G will be to find solutions as smart and flexible as possible while maintaining low complexity.

1.5 New Radio (NR)

New Radio (NR) is the Radio Access Technology (RAT) defined by 3GPP for 5G. An intermediate release of NR was already available by the end of 2017 (3GPP release 15), in order to target some markets needs, in the form of non-standalone system. In these systems LTE still plays the role of primary communication technology, providing wide area coverage and control plane management, while NR provides support to reach higher data-rates.

To completely exploit the benefits of all the new technologies composing NR, the technical work proceeded to define the specification for a standalone solution in release 16 (confirmed in June 2018). The actual implementation of course takes longer, but it should be now imminent.

One of the main 5G systems developers, Ericsson, on the 6th July 2020 announced that: "Communications service providers can now tap the full potential of 5G New Radio (NR) technology with the commercial availability of Ericsson (NASDAQ: ERIC) Standalone 5G NR software for 5G mid and low bands" [12].

Clearly NR RAT must be suitable for supporting massive MIMO and the new spectrum, but not only. In the next sections some of the other main components of NR are reported².

1.5.1 Waveform

The signal modulation in LTE is based on Cyclic Prefix - Orthogonal Frequency Division Multiplexing (CP-OFDM).

²Notions mainly found in [11] and in [21]

Orthogonal Frequency Division Multiplexing (OFDM) is a particular technique of Frequency Multiplexing which divide the allocated bandwidth in many subcarriers, small enough to consider the frequency response inside them as flat. This way, frequency selective fading is no longer a problem. Moreover, the subcarriers can be packed together using the frequency domain orthogonality of properly spaced sinc-square functions (an example in figure 1.6), simple to realize in time domain through rectangular shaped pulses.

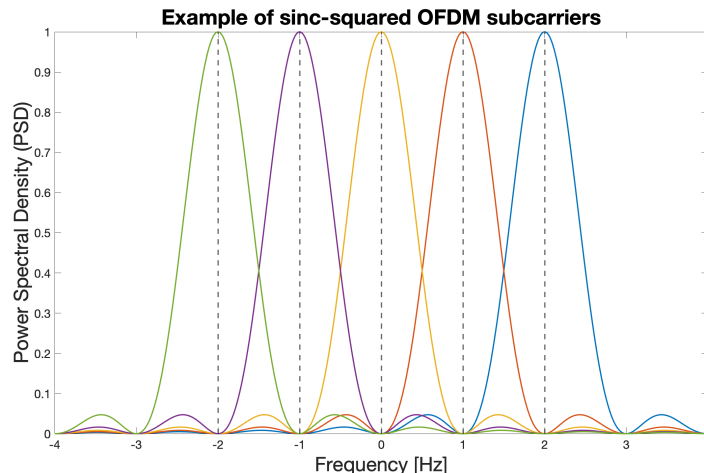


Figure 1.6: Example of the frequency domain orthogonality of sinc-squared per-subcarrier spectrum.

Cyclic Prefix is introduced to avoid the Inter Symbol Interference (ISI) caused by the reception of different reflected replicas at the receiver side. It occupies the first fraction of the OFDM symbol (approximately 7% of the total), obtained from a copy of the last part of the symbol itself, to maintain the orthogonality condition.

For NR different kinds of waveform have been proposed and studied, in order to get rid of a particular problem of OFDM. This drawback resides in the relatively high side-lobes power generated by the sinc-square shaped per-subcarrier spectrum: CP-OFDM requires relatively high guard bands at the edges of the frequency interval, in order to avoid interference among adjacent bands. In LTE, considering a band of 20 MHz, the guard bands occupy as much as 2 MHz, so the frequency efficiency drops to 90%.

The main challenge is then to preserve the advantages of CP-OFDM while improving the frequency efficiency. This problem is mostly addressed to lower frequencies bands (below 6 GHz), since at higher frequencies the capacity is for sure not a problem, at least for now. Different solutions have been proposed and studied, as CP-OFDM with windowed overlap-and-add (WOLA) processing, universally filtered multicarrier (UFMC), and filtered orthogonal frequency division multiplexing (f-OFDM). They use different techniques but with the same goal, i.e. reduce the amplitude of out-of-band signal power, thus improving spectrum confinement.

Since they all are based on conventional CP-OFDM, and one of the NR specification

is to be future-proof and flexible, the agreement is on a "new transparent waveform processing approach" [21]: at below 52.6 GHz, the system relies on CP-OFDM-based waveforms. This means that the particular waveform processing at the transmitters and receivers side can be different, allowing ad-hoc solutions. The developers are then permitted to design each system with a certain level of freedom, considering the trade-off between the need of more spectrum and the increased complexity.

Moreover, while in LTE the chosen waveform for the uplink was the Single Carrier-FDM (SC-FDM, or DFT precoded OFDM) only, in NR both downlink and uplink employ the same transparent waveform paradigm, with the constraint for UEs of supporting SC-FDM (while it is optional for BSs). SC-FDM is useful for the device power efficiency since it limits the peak-to-average power ratio (PAPR), given the low power budget of the UE Power Amplifier (PA). It is similar to OFDM, but the allocated band is composed by adjacent subcarriers. It is named also DFT-precoded OFDMA because symbols are precoded with a DFT before the OFDM modulation. The NR choice is in line with the concept of offering flexibility to individual usage situations.

Considering frequencies above 52.6 GHz, further studies have to deal with the lower of PA efficiency and the complexity constraints.

1.5.2 Multiple access and numerology

OFDM-based waveform permits a simple but convenient multiple access technique: Orthogonal Frequency Division Multiple Access (OFDMA). Defined in LTE, OFDMA organises the frequency and time resources in a resource grid (figure 1.7):

- Time axis is divided in frames of 10 ms. Each frame is composed by 10 subframes (or Time Transmission Interval TTI) of 1 ms. Inside a subframe 14 OFDM symbols are transmitted.
- Frequency domain is divided in subcarriers of 15 kHz.

The pair composed by both time and frequency is then represented by the Resource Elements (RE), i.e. a single OFDM symbol over one subcarrier, and the Resource Block (RB), a frequency-time grid of 12 sub-carriers ($180 \text{ kHz} = 12 \cdot 15 \text{ kHz}$) and 1 TTI (i.e. 14 OFDM symbol). The RB is the smallest amount of resources that a UE can be assigned to.

NR is still based on this OFDMA scheme, but it has to deal with a wider range of frequencies, where the key targeted channel characteristics changes. It introduces the support for multiple OFDM numerologies, corresponding to the parameter μ , setting the Subcarrier Spacing (SCS) Δf , ranging from 15 kHz up to 240 kHz with a proportional change in cyclic prefix duration [11] (table 1.1). The relation is:

$$\Delta f = 2^\mu \cdot 15 \text{ KHz}$$

In the time domain a new concept of *slot* is introduced: it corresponds to 14 OFDM symbols but, while the subframe has a fixed duration of 1 ms, the slot duration depends on the numerology, considering that the OFDM symbol duration is inversely

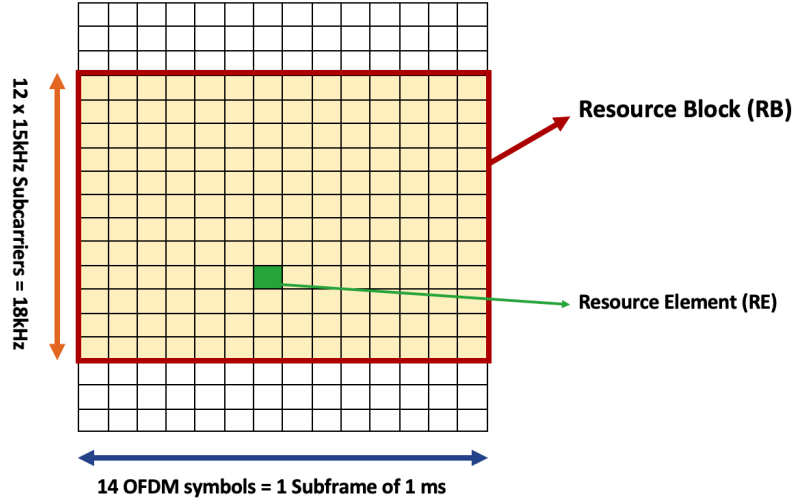


Figure 1.7: LTE OFDMA Time/Frequency resource allocation.

μ	Δf [kHz]	Frequency Range	Slot duration [ms]	Cyclic Prefix
0	15	FR1	1	Normal
1	30	FR1	0.5	Normal
2	60	FR1, FR2	0.25	Normal, Extended
3	120	FR2	0.125	Normal
4	240	FR2	0.0625	Normal

Table 1.1: Relation between numerology and SCS.

proportional to the SCS:

$$\text{Slot length} = \frac{1 \text{ ms}}{2^\mu}$$

Consequently one subframe can contain more slots, from just 1 up to 16.

Higher numerologies are meant to be used at higher frequencies, where wider bandwidths are available, and shorter slots are useful in order to lower the latency. Transmissions at higher frequencies could also suffer from larger carrier frequency offset and phase noise, that can be contrasted by higher SCS. It is important to note that the Cyclic Prefix shortening does not translate into ISI, since at higher frequencies the cell coverage is smaller and so the maximum delay between the signal and its reflected replicas is smaller too.

However, the goal represented by low latency transmissions must also be satisfied with lower numerologies. Therefore, NR introduces a new kind of time partitioning called "mini slots": a single slot can be further divided into smaller subsets of OFDM symbols. This solution is more complex but very efficient for small messages exchange, since the receiver does not have to wait the slot start instant before going on with the processing. Buffering is one of the main latency component, and mini slots seek then

the reduction of its negative impact.

1.5.3 Duplex Schemes

Duplex Schemes represents a key design aspect in wireless communications, deeply affecting the transceiver operation. In LTE the most common solution is a paired spectrum allocation with Frequency Division Duplexing (FDD): transmitter and receiver can simultaneously access the channel, but in different frequency intervals, sufficiently spaced apart. However, Time Division Duplexing (TDD) with unpaired spectra could ease the channel estimation, since both the communicating terminals sense the channel in the same frequency range, not possible with FDD, where frequency-selective fading results in different channel behaviour along frequency axis. In figure 1.8 both TDD and FDD are represented in a simplified way.

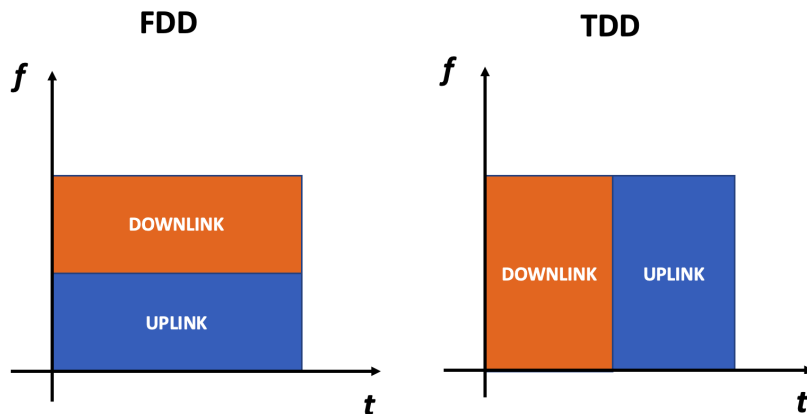


Figure 1.8: Simple representation of FDD and TDD schemes.

In LTE they were both supported, but with two different frame structures. The solution of NR is to exploit both the duplexing scheme, but with a unique frame structure, and also enhancing the importance of TDD. TDD is particularly useful in the dense small-cells scenario, where the load balance between downlink and uplink can quickly change (high variability in the number of users).

The mini slots previously defined can be used to support TDD by allocating subsets of OFDM symbols inside a slot to both to uplink(UL) and downlink(DL), in a static, semi-static or dynamic way. It follows a better usage of the available resources, thanks to traffic adapting schedulers, but the complexity tradeoff must be advantageous (and it is not always so, it depends on the particular scenario).

TDD introduces strict requirements in the time synchronization within both the UE-BS link but also inside the network, to avoid intercell interference and guarantee transmission coordination. Transceiver switching time from transmitting to receiving mode in TDD is also another issue vendors must carefully design.

1.5.4 Ultra-Lean Design

The impact of the energy consumption of telecommunication networks has acquired increasing interest over the years. As early as the end of 2012, the contribution to global electricity consumption was estimated around 1.8%, with a tendency to grow by 10% every year[13]. Numbers not to be underestimated.

Energy efficiency is a key issue also in 5G, which needs the implementations of new systems, as for example the installation of numerous new small-cells and micro-cells, thus increasing the demand for energy resources.

To counter this negative impact, both from an environmental and cost point of view, for mobile operators and service providers, NR seeks to minimize the generation and transmission of unnecessary signals. In mobile networks a subset of resources is usually assigned to signals and physical-layer control channels to support communication with the UEs. They give important information about the system and reference signals can be used for channel estimation. The problem in LTE is that there is no adaptation to the actual presence or absence of devices in the cell, leading to a waste of transmissions ("always-on" signals). A subset of these signals and channels is intended for the initial access and synchronization, deepened in the next chapter and of main interest in this thesis.

The "Ultra-Lean Design" then corresponds to a smarter resource management, by minimizing the waste of resources by non-data signals. A reduction in inter-cell interference is also achieved, thus obtaining higher data-rates.

1.5.5 Backward and forward compatibility

As with non-standalone 5G systems, interoperability with LTE has proven to be of particular benefit. In the future, depending also on cost-benefit studies, NR may decide to rely on LTE or NR itself for lower frequency communications. Interworking between the two must be guaranteed, in order to provide the best coverage as possible, difficult task at mm-Waves, and a transparent procedure to the user.

The NR specifications have been designed to allow also a simpler future evolution, for the implementation of new technologies that do not require major changes to the general structure. It is not a simple definition to obtain, but it can be partly guaranteed by the absence of stringent specifications on the predetermined allocation of time/frequency resources, thus leaving some degrees of freedom.

1.6 Network slicing

From [15]: "Network Slicing (NS) refers to the managed partitions of physical and/or virtual network resources, network physical/virtual service functions that can act as an independent instance of a connectivity network and/or as a network cloud. Network resources include connectivity, compute, and storage resources".

A network slice can be seen as a single end-to-end logical network, composed by a subset of physical and/or virtual network elements from the overall underlying network. Its

creation takes place according to the particular needs and use cases, taking into account the characteristics of the services for which it will be used. Network slicing is the result of the combination of two new network paradigms:

Software Defined Network (SDN) Traditional computer networks are based on closed platforms, i.e. network nodes with huge computational capabilities but with vendor specific interfaces, high costs and usually difficult customization. Moreover, there is a no clear separation of control plane and data plane, and the management plane does not provides a lot of automatised algorithms and usually needs human intervention. SDN tries to deeply renew the traditional architecture with some new key elements:

- A common and simple interface (API) between data and control plane.
- Simple programmable switches with only forwarding function (general purpose HW), relying on a logically centralized control plane with a global network view.
- Flow based switching able to quickly adapt to the traffic and to link outage (no need of distributed algorithms), with simple packet-handling rules.

SDN controller is the central point of the network, on which the actual networking applications are installed. Working mostly on this single network node and not on all the other switches/routers etc. permits an easier and faster innovation via software updates, but also a more precise monitoring for traffic control, billing and Inter-cell Interference Management.

Network Function Virtualisation (NFV) New market demands are pushing for dynamic and service-aware networks, which performance and costs are tightly related to the particular service. In order to accomplish these demands, NFV can be employed. Virtualization refers to the abstraction of resources, performed by the SDN controller, through a description that depends on properties that match certain predefined selection criteria. NFV defines network functions implemented in software, called Virtual Network Functions (VNFs), based on these abstracted resources. The next step is the definition of Network Services, realized with a combination of VNFs, that are thus independent from the actual hardware devices composing the network. A NFV orchestrator is in charge of the management of the entire structure, allocating the required services and resources.

Network slicing aims then the request of smart networks, enhancing the mobile communications impact in business processes and customer-specific services, giving the operators new economic solutions in the Business to Business segment [15]. It is also one of the main component of the new 5G core network (5GC), the part of the overall network architecture providing functions of upper layers than the radio access. 5GC is based on LTE's Evolved Packed Core (EPC), but more specifically targets the service requested by the user's application side.

Chapter 2

Initial access and synchronization procedure for an NR receiver

One of the most critical operation to guarantee the good behaviour of the overall mobile network is the synchronization procedure between UE and BS.

Since the UE is not aware of the reachable transmitting BSs inside its range before establishing a connection, it must perform a cell search. At the initial stage, considering for example a device just turned on, it should start to analyse the on-air signal to detect the presence of one or more transmitting antennas. The information recovery on surrounding cells needs some ad-hoc signals and channels, designed to be robust against harsh environments. The receiver must also take into account some technology-intrinsic impairments, like time and frequency misalignment w.r.t. the system reference. This is caused by the clock inaccuracy affecting any oscillator, which leads to misalignment with the timing and frequency of the mobile network. Errors of this kind could severely disrupt the communication. For example, in GNSS systems, errors in timing reference of few micro seconds can lead to hundreds meters of errors.

The synchronization is then a particular phase necessary to correctly detect the cells and apply the correction in frequency and time alignment. Another cell search purpose is to provide mobility to system users, continuously checking for new and better communication serving cells, and then to decide if an handover becomes necessary.

A distinction can be made when the device is already in connected-state or in idle/inactive-state, since in the first state the network could simplify the operation by providing the user with useful system information.

2.1 Synchronization in the past mobile networks

Synchronization is part of the physical layer, backbone of any new wireless technology, which evolution moves on together with the available technology and requirements.

Looking at the mobile standards history, the synchronization issue has always been studied, producing many different methods, often with different targets and requirements.

For 1G, the synchronization had to solve the problem of interference from adjacent channels, and the realization of a coherent demodulation in wide-band FM. This required a technique capable of correcting the carrier phase shift.

Thanks to the transition to digital communications with 2G, new techniques became available, exploiting the channel coding to obtain symbol timing synchronization and adaptive equalization techniques.

The introduction of 3G wider-band transmissions increased the requirements to suppress multiple access interference (MAI). Pseudo-Noise (PN) codes with 64 chips length were used to achieve slot synchronization, frame synchronization, and frequency acquisition.

With the transition to an OFDM modulation, the introduction of MIMO and other advanced techniques, 4G carried on new studies on initial access. Time, frequency and phase synchronization were still essential for the system, but new codes and signals had to be designed.

LTE (and in particular LTE-A) results are the foundation upon which 5G solutions are built, taking into account the new usage cases, each with its particular requirements. Thus flexibility recurs also in 5G synchronization design, together with new demands of energy efficient technologies¹.

2.2 The SS-Block

In LTE systems a two special signals and one physical channel have been defined to perform synchronization. They are the Primary Synchronization Signal (PSS), Secondary Synchronization Signal (SSS) and a Physical Broadcast Channel (PBCH) with its Demodulation Reference Signal (DMRS), jointly indicated as LTE PSS/SSS/PBCH.

The evolution with respect to the LTE PSS/SSS/PBCH implementation resides in the demand of a faster and more accurate radioframe synchronization for the UEs. An improvement of time and frequency offset estimation and correction is also desirable considering the forthcoming bands at higher frequencies, which result in large values of frequency and time offsets. This would counteract the arising of Inter Carrier Interference (ICI) and ISI, possibly supported by the employment of more accurate (but also more expensive) oscillators at transmitter and receiver side [19].

Firstly 5G takes LTE PSS/SSS/PBCH to build a single structure called Synchronization Signal Block (SSB), periodically transmitted on the downlink by each NR cell to perform the synchronization procedure: devices can understand they are inside the coverage area of a cell by finding the SS-Block. It occupies a total amount of 960 resource elements in the OFDM grid: 4 OFDM symbols in time domain and 240 contiguous subcarriers (20 RBs) in the frequency domain, for each symbol. The actual band in

¹Adapted from [18]

Hz and time duration in sec of the SS-Block depends on the numerology adopted by the network.

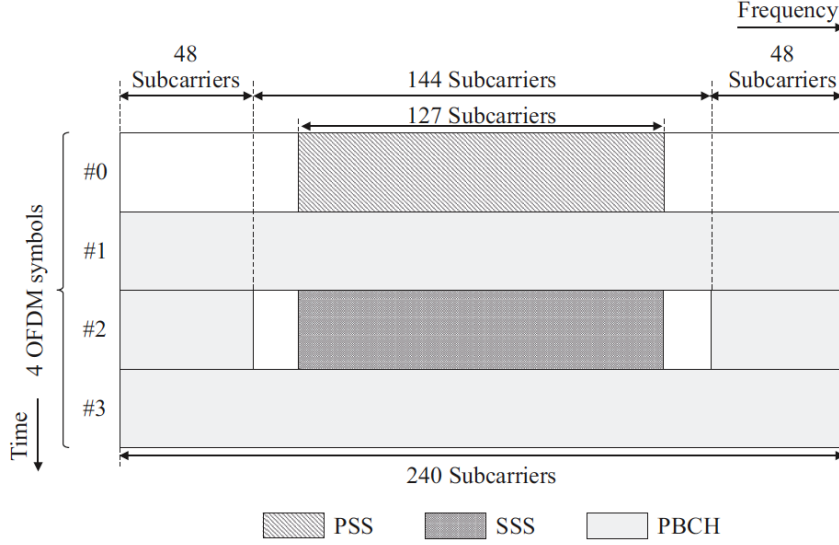


Figure 2.1: SS/PBCH block structure [28].

Channel or signal	OFDM symbol number / relative to the start of an SS/PBCH block	Subcarrier number k relative to the start of an SS/PBCH block
PSS	0	56,57, ..., 182
SSS	2	56,57, ..., 182
Set to 0	0	0, 1, ..., 55 183, 184, ..., 239
	2	48, 49, ..., 55 183, 184, ..., 191
PBCH	1, 3	0,1, ..., 239
	2	0,1, ..., 47 193, ..., 239
DM-RS for PBCH	1, 3	$0 + v, 4 + v, 8 + v, \dots, 236 + v$
	2	$0 + v, 4 + v, 8 + v, \dots, 44 + v$ $192 + v, 4 + v, 8 + v, \dots, 236 + v$

Table 2.1: Resources within an SS/PBCH block for PSS, SSS, PBCH, and DM-RS for PBCH [22].

The SS-Block structure is reported in figure 2.1, with the disposition of the two SS and the PBCH channel.

The PSS occupies the middle 127 subcarriers in the #0 OFDM symbol, while the other

symbol's subcarriers are left unallocated.

The SSS, like the previous one, requires 127 subcarriers in the central frequency band of the #2 OFDM symbol, with a guard band of respectively 8 and 9 empty subcarrier on each side.

PBCH is transmitted over the left frequency resources in the #2 OFDM symbol (48 on the left and 48 on the right side subcarriers), and it is transmitted also over the entire #1 and #3 symbols, within its associated DM-RS.

This multiplexing scheme is valid for all 5G systems, but other parameters can be managed depending on the application scenario.

One of them is the SSB transmission **periodicity**, differing from LTE where each PSS/SSS couple is transmitted every 5ms. In order to actualize the ultra-lean design principle of 5G, the periodicity of the SSB can assume values from the set: $T_{SS} = 5; 10; 20; 40; 80; 160$ ms. Longer time intervals means less amount of always-on signals, decreasing the interference between adjacent cells and the control signal overhead. The downside is represented by the longer time the device must wait in order to conclude that there is no SSB in a certain frequency.

To limit the waste of time for devices in initial cell search or in inactive/idle state, the SSB periodicity is assumed by the User Equipment to be 20 ms at maximum.

To speed up the cell search another solution is adopted, by the definition of a **synchronization raster**: only a limited set of frequencies can be used to transmit the SSB, within each frequency band. It is an evolution from LTE, since the PSS and SSS were always located at the center of the carrier. Its advantage was the inherently determination of the center frequency of the carrier, but the drawback was that many carrier positions are possible (large *carrier raster*), extending the searching duration. In 5G the SS-Block can be placed in any frequency of the synchronization raster, not only in the center of the carrier, and it could also not even be aligned with the resource-block grid. The PBCH is then in charge of giving some information about the exact SSB frequency-domain position within the carrier [20].

The previous defined periodicity is not actually referred to a single SSB, but to a **SS-Block Burst Set**. It is composed by multiple SS-Blocks, allowing flexible resource allocation and beamforming, always confined to a 5 ms time interval, either in the first or second half of a 10 ms frame. When beamforming is present at the transmitter side, the Burst Set can be further divided into groups of one or many SSBs, each then assigned to a certain beam (figure 2.2).

The time-domain organization of the Burst Set is based on a Time Division Multiplexing (TDM) scheme, chosen from a given collection. The maximum number of SS-Block transmissions per SS-Block burst set depends on the carrier frequency range [21]:

- $L_{MAX} = 4$ locations available at below 3 GHz;
- $L_{MAX} = 8$ locations available between 3 and 6 GHz;

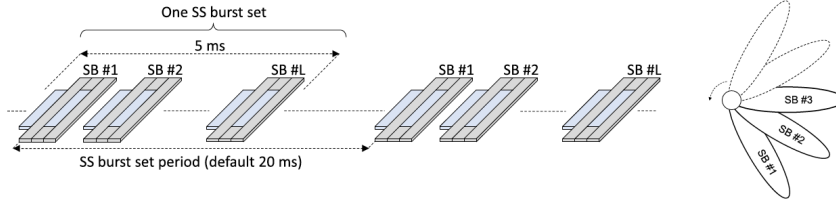


Figure 2.2: Multiple time-multiplexed SS blocks within an SS-burst-set period [20].

- $L_{MAX} = 64$ locations available at above 6 GHz;

The decision on whether to use all the available locations or not, and on which fixed TDM scheme to be employed for the SS-Blocks, depends on the numerology adopted by the system: longer duration of the OFDM symbols (i.e. smaller numerology μ) means longer SS-Blocks overhead inside a frame, which should be avoided.

The maximum number of SS-Blocks corresponds also to the maximum number of possible beams for the beam sweeping, which is particularly useful for higher frequencies, where more beamforming gain is needed to counteract path loss.

Different metrics can be used to select the best beam by the UE, which then will correspond to the transmission occasion time interval for the actual connection with the network. For example the Reference Signal Received Power (RSRP) given by the DMRS detection (associated with the PBCH) or the Reference Signal Reported Quality (RSRQ), given by SSS, can be exploited for the beam measurement [19].

2.3 Primary Synchronization Signal (PSS)

The Primary and Secondary synchronization signals permit the determination of the Physical Cell Identity (PCID) of the cell. In NR radio interface PCID can assume 1008 different values. Called also N_{ID}^{cell} , is given by the combination of the cell identity group index $N_{ID}^{(1)}$ ($\in \{0, 1, \dots, 335\}$) and the physical-layer identity within the cell-identity group $N_{ID}^{(2)}$ ($\in \{0, 1, 2\}$). The relation is [22]:

$$N_{ID}^{cell} = 3N_{ID}^{(1)} + N_{ID}^{(2)} \quad (2.1)$$

The PSS sequence is the first synchronization signal inside the received SSB and also the first signal the UE searches for.

Its purpose is to define the initial symbol alignment and apply a coarse frequency correction, since at initial access stage the system timing is not available and the UE oscillator inaccuracy could produce a mismatch with the system reference carrier frequency. Neither system numerology and SCS are available, so the PSS detection in frequency bands with two SCS options must be performed through a blind search, to

check both options.

NR PSS is a FDM-based BPSK M-sequence of 127 elements, thus occupying 127 subcarriers, out of the 240 of the SS-Block band. Differently from the SSS, all the remaining SSB subcarriers in the same OFDM symbol are used as guard band, so they are set to 0.

There are three different possible sequences x_0 , x_1 and x_2 , depending on the three different values that N_{ID}^2 can assume. The sequence $d_{PSS}^{(l)}(n) (l = N_{ID}^2)$ for the PSS is defined by [22]:

$$\begin{aligned} d_{PSS}^{(l)}(n) &= 1 - 2x(m) \\ m &= (n + 43N_{ID}^2) \bmod 127 \\ 0 &\leq n \leq 127 \end{aligned} \quad (2.2)$$

Where polynomial $x(i)$ is given by the recursive formula:

$$x(i + 7) = (x(i + 4) + x(i)) \bmod 2 \quad (2.3)$$

And it can be computed from its initial values, specified as:

$$[x(6) \ x(5) \ x(4) \ x(3) \ x(2) \ x(1) \ x(0)] = [1 \ 1 \ 1 \ 0 \ 1 \ 1 \ 0]$$

The resulting three PSS sequences are then the result of a basic M-sequence cyclically shifted.

Also in LTE there were 3 possible PSSs, but they are Zadoff-Chu sequences with a length of 62. The switch to M-sequences is motivated by the time and frequency offset ambiguity affecting Zadoff-Chu sequences: the correlation function outputs undesired periodical peaks along frequency axis, and side peaks along time axis (figure 2.3).

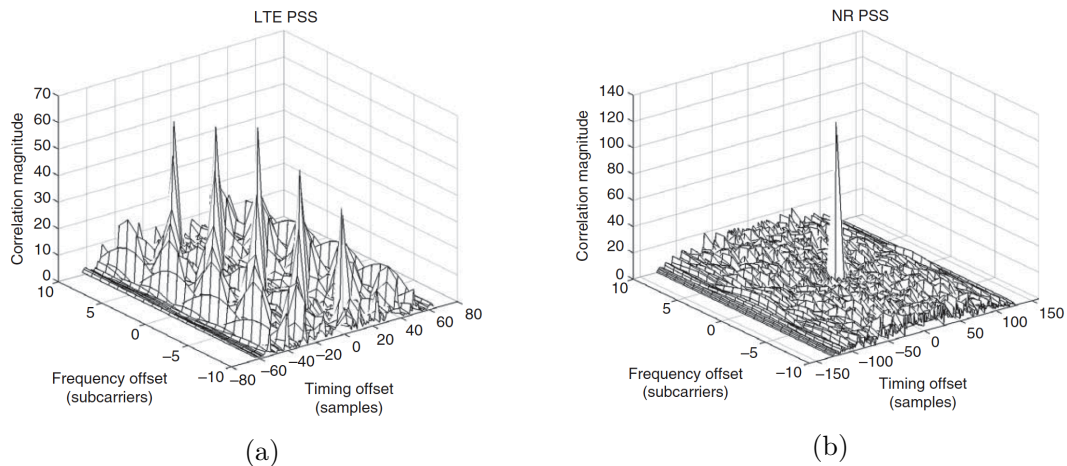


Figure 2.3: PSS time and frequency offset ambiguity of (a) LTE PSS sequence (left) and (b) NR PSS sequence (right) [21].

5G then allows the estimation of the frequency offset in one-shot, while in LTE from PSS detection there would be a set of candidates equispaced in frequency. Doubling the sequence length results also in a 3 dB larger processing gain, due to the higher peak with respect to the correlation noise floor. The drawback is the need of longer filters at the receiver side, implying an increase in complexity.

At receiver side, PSS detection is performed to get the actual PSS transmitted sequence out of the possible three, and so $N_{ID}^{(2)}$ is automatically found. Auto-correlation or cross-correlation are the common operations used for detection. Due to the absence of system information and time/frequency corrections, PSS detection must be the most robust operation with respect to SINR-level and to relatively large carrier frequency deviations between the UE and gNB. Moreover, it must be performed in time domain, since the OFDM demodulator cannot apply the FFT without the corrected OFDM symbols time alignment².

2.4 Secondary Synchronization Signal (SSS)

Secondary Synchronization Signal (SSS) definition is based on $N_{ID}^{(1)}$, which is used to distinguish between different cells, and not for the 3 different sectors inside the same site, as in the case of $N_{ID}^{(2)}$.

M-Sequences have very good auto correlation properties, but suffer of bad cross correlation properties if the M-sequences are generated by different Linear-Feedback Shift Register (LFSR) circuits. A different solution is then chosen: Secondary Synchronization Signal (SSS) is a Gold Sequence with chip length of 127, obtained by the combination of two M-sequences, solving the cross correlation problem.

The sequence $d_{SSS}^{(j)}(n)$ ($j = N_{ID}^{(1)}$) for the secondary synchronization signal is defined by [22]:

$$\begin{aligned}
 d_{SSS}^{(l,j)}(n) &= [1 - 2x_0((n + m_0) \bmod 127)] \cdot [1 - 2x_1((n + m_1) \bmod 127)] \\
 m_0 &= 15 \left\lfloor \frac{N_{ID}^{(1)}}{112} \right\rfloor + 5N_{ID}^{(2)} \\
 m_1 &= N_{ID}^{(1)} \bmod 112 \\
 0 &\leq n \leq 127
 \end{aligned} \tag{2.4}$$

where x_0 and x_1 are functions defined as:

$$\begin{aligned}
 x_0(i + 7) &= (x_0(i + 4) + x_0(i)) \bmod 2 \\
 x_1(i + 7) &= (x_1(i + 1) + x_1(i)) \bmod 2
 \end{aligned} \tag{2.5}$$

²Adapted from [20] and [21]

x_0 and x_1 assume the same initial values:

$$[x_0(6) \ x_0(5) \ x_0(4) \ x_0(3) \ x_0(2) \ x_0(1) \ x_0(0)] = [0 \ 0 \ 0 \ 0 \ 0 \ 0 \ 1]$$

$$[x_1(6) \ x_1(5) \ x_1(4) \ x_1(3) \ x_1(2) \ x_1(1) \ x_1(0)] = [0 \ 0 \ 0 \ 0 \ 0 \ 0 \ 1]$$

The possible SSS transmitted candidates are 336. They depend on the 1008 value of PCIDs, but $N_{ID}^{(2)}$ is recovered from the PSS, so the actual amount of possible SSSs are decreased by a factor of 3. The SSS is located in the 127 central subcarriers of the #2 SSB's OFDM symbol, identified at the receiver side from the PSS position.

Since time and frequency grid should be correctly managed after PSS detection, the SSS processing by the device can be performed in the frequency domain, after the FFT. This permits a lower computational complexity, avoiding computation of the correlation for all the possible delay of the slot.

2.5 Physical Broadcast Channel (PBCH)

The Physical Broadcast CHannel is a physical channel used to provide the very first system information:

- System Frame Number (SFN): similar to LTE, NR does have a 10 bit System Frame Number starting from 0 to 1023 (for timing purposes);
- Half frame bit indicator and Most Significant Bits (MSBs) of the SS Block position within an half-frame (SS-Block time index);
- Master Information Block (MIB): a minimum amount of system information including also how to receive Remaining Minimum System Information (RMSI). Parameters for receiving RMSI provide the UE with information about time and frequency resources of COntrol RESource SET (CORESET) and monitoring parameters like periodicity and window duration for detecting Physical Downlink Control CHannel (PDCCH) ,that schedules Physical Downlink Shared CHannel (PDSCH), carrying the actual RMSI data.

MIB information is received by the physical layer after its generation at higher levels, consisting in one transport block of $\bar{A} = 24$ bits (at maximum) every Transmission Time Interval (TTI) of 80 ms. Before the transmission through the radio channel, it is processed in several steps ([24] [22]):

Payload generation The MIB is extended by some timing related bits: 4 bits from Last Significant Bits (LSB) of SFN, the 1 bit of half frame bit, and 3 additional bits which value depends on the Frequency Range (FR). Its length is thus: $A = \bar{A} + 8 = 32$ bits. The payload is then subjected to an interleaving operation, to improve the PBCH polar decoder performance and latency.

First Scrambling operation PBCH payload is masked (scrambled) with a sequence which shall be initialized with the Cell ID N_{ID}^{cell} and the 3rd and 2nd LSB bits of SFN (s2, s1) carried in the payload. To allow the user determine the applied mask upon successful Polar decoding, in order to reverse scrambling operation, SFN bits (s2, s1), half-frame bit (s0) and SS-Block index (b5, b4, b3) remain unmasked. The goal of the scrambling is to obtain randomization of the intercell interference by varying the payload along time with SFN bits, that change every 20 ms.

Transport block CRC attachment A Cyclic Redundancy Code (CRC) of length $L = 24$ bits is added to the BCH transport blocks in order to detect errors over the transmitted bits. The L CRC parity bits are computed on the entire transport block, using the generator polynomial $g_{CRC24X}(D)$. The total length of the sequence becomes $B = A + L = 32 + 24 = 56$ bits.

Channel encoding and Rate matching Polar coding is the channel encoding technique adopted for PBCH transmission. It is based on a recursive structure with quite low complexity, base on the principle of "Channel Polarization": starting from a single channel, it is possible to derive N copies of it among which some of them are completely noiseless while other completely noisy. Decoding relies on Successive Cancellation and List Decoding³.

At the output of the encoder the sequence generated is $N = 2^{nmax} = 2^9 = 512$ bits long.

A Rate Matching block then applies bit repetition to obtain a sequence of length $E = 864$ bits, with $E > N$.

Second Scrambling operation After encoding an additional scrambling based on Cell ID is applied to keep the channel coding procedure similar between physical channels.

Modulation and mapping to physical resources The modulation for PBCH is a QPSK modulation, which outputs a block of complex valued modulation symbols. The last PBCH-specific processing is the mapping of the modulation symbols into the time and frequency resources, i.e. the RBs within the SSB. The correct allocation has already been presented.

Thanks to the linearity of CRC calculation and linearity of the PBCH encoding process, at the receiver side soft combination of PBCH over multiple SS-Blocks can be performed. This is particularly useful for very low SINR scenarios, for example for devices at the edge of the cell coverage, where single shot detection could fail.

Soft combination can be divided into intra-burst soft-combining and inter-burst soft-combining, and in both cases the receiver must compensate for the particular differences in the payload between different SS-Blocks.

³More on Polar Codes in [26]

2.5.1 Demodulation reference signals (DMRS) for PBCH

DMRS is introduced to permit the coherent demodulation of PBCH at the UE, since it is designed for radio channel estimation. In [22], section 7.4.1.4, the definition of the reference-signal sequence is reported.

During the mapping of PBCH in the RB grid, its associated DM-RS is mapped too, following the rule $N_0 + v, N_0 + 4 + v, N_0 + 8 + v, \dots$ (in detail in table 2.1) for the index of subcarrier number k , relative to the start of the SS/PBCH block. The frequency shift in the frequency position of DM-RS is determined by v , which is given by $v = N_{ID}^{cell} \bmod 4$. This value depends on the cell ID, which can be derived in advance by PSS and SSS detection. For this reason the DM-RS sequence can be localized by the receiver within the SS-Block, allowing the further process of PBCH recovery. The actual transmitted sequence can be found through the cross-correlation function with a list of local replicas of DM-RS sequences.

The detection can be realized in either a coherent or non-coherent way⁴. The coherent detection is implemented whether the received sequence has been firstly compensated for phase and amplitude variations introduced by the channel (for example using SSS as a phase reference). It assures better performance than the non-coherent case, but an increased complexity.

The detection of the sequence provides the LSB part of the SS-block index, thus making each SS-block decodable independently from the others.

In figure 2.4 a block scheme represents the detection of the SS-Block from the user point of view.

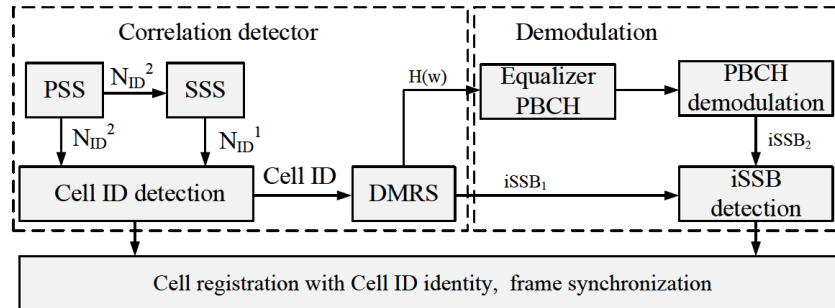


Figure 2.4: Radioframe synchronization procedure [23].

2.6 Providing remaining system information

System information can be distinguished between the essential information for the device access to the network (SIB1 or RMSI), or the information that could be get

⁴More details in [25]

after the connection establishment. In LTE, both kind of system information were periodically broadcast, while for 5G NR there is the possibility to transmit the second kind on demand, i.e. only after an explicit request, to avoid the waste of resources.

As explained before, SS-Block provides only a small amount the overall information, but from the PBCH decoding the UE can locate the PDSCH transmission (which has periodicity of 160 ms) within the frequency/time grid, containing the RMSI⁵.

RMSI is very important because its information makes the UE able to perform the initial random access.

2.7 Random Access

Random Access is the last procedure the UE has to perform within the initial access, once it get the knowledge of being inside the coverage of one or more cells. It is a particularly critical stage in NR, since it has to deal with beamforming and ultra-dense networks that have to be able to satisfy a huge amount of connected devices.

Random Access techniques for mobile techniques have largely been studied, and tried to be continuously improved, since collision during initial access can largely drop the network performance.

It is not analysed with tests and simulation in this thesis, so only a brief description is reported here.

The Random Access is performed over the selected beam, i.e. the beam with the highest signal received power. Cell RACH resources are required by the device to start the procedure, and they become available after the SIB decoding. The UE exploits this information to transmit a RACH preamble (Message 1) on the configured RACH resources. If gNB correctly receives Message 1, it responds with a random access response (RAR, Message 2), followed by a RRC connection request (Message 3). Finally, the UE sends to the a RRC connection setup complete (Message 2) to the gNB.

Once RA procedure is completed, a dedicated connection is established between UE and gNB with its dedicated connection ID [19].

A complete representation of the initial access synchronization stage is shown in figure 2.5.

⁵Adapted from [20]

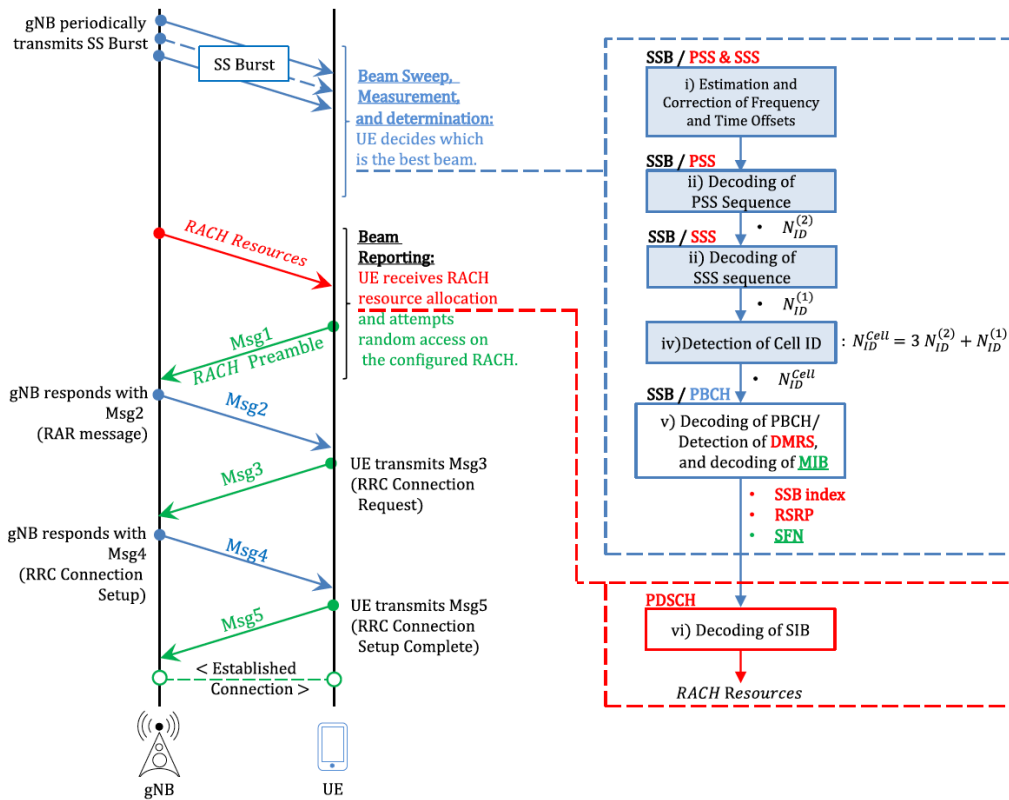


Figure 2.5: 5G NR synchronization procedure [19].

Chapter 3

Description of TIM Physical Layer simulator

Simulators play a fundamental role in the process of developing new technologies. They allow testing, performance evaluation and critical issues detection of the studied algorithms and techniques, before going on with the actual implementation. A realistic and complete simulator can therefore also be the main deterrent of costly interventions and modifications of a system.

Even in mobile networks simulators are widely used, considering the large amount of variables that can characterize a system of this type (environment, available resources, traffic level, atmospheric conditions, etc.).

The 3GPP standardization body tests and optimizes the new algorithms and procedures using simulators, which are traditionally divided into:

- **Link Level simulators**, that simulate a single link between a transmitting node and the receiving node, particularly focusing on the physical layer processing carried out at the transmitter and the receiver, as well as the effects of the channel on the transmitted waveform.

This usually results in very computational intensive simulation, but they can provide valuable insight on the merit of different solutions and techniques, understanding which solution is the most promising for a given scenario or objective.

Link Level simulation results are usually provided in terms of certain Key Performance Indicators (e.g. Throughput, Block Error Rate - BLER, Bit Error Rate - BER) as a function of the simulated Signal to Interference plus Noise Ratio (SINR) for a given channel propagation condition.

- **System Level simulators**, that simulate a whole network, with several transmitting nodes that transmits to several receivers. To keep the computational complexity at a reasonable level, each link is represented through abstraction models that simplify the actual complexity of the physical transmission (this abstraction models are usually obtained through link level simulations).

In this thesis the objective is the evaluation of the synchronization process during the initial access, from the point of view of a receiving node, given the transmission of the SS-Block by a BS, i.e the transmitting node (communication point-to-point). For this reason the simulator used is a Link Level type, developed in the TIM laboratories mainly with MATLAB, while some blocks, particularly critical from the point of view of execution time, are implemented in C language and recalled by MATLAB via MEX. Its purpose is to model a radio interface that complies with the 3GPP specification for the 5G standard.

It implements a complete transmission chain with several modules that simulate the processes of a real transmitter as the signal generation and modulation, the behaviour of the wireless channel, and the processes carried out by the receiver to retrieve and decode the data and signals.

Different 5G New Radio Physical Channels have been already implemented in the simulator, as well as the generation of the SSB.

In figure 3.1 the transmission chain for the Physical Downlink Shared Channel (PDSCH) is shown.

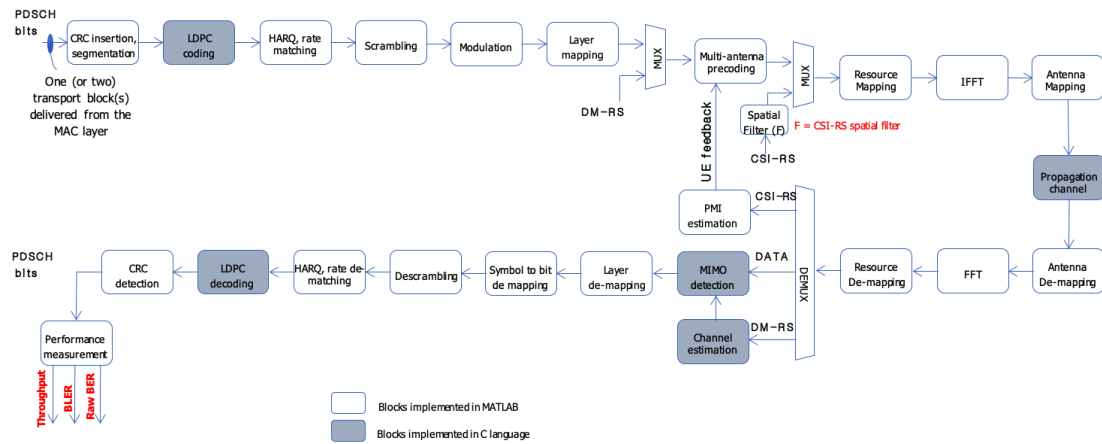


Figure 3.1: 5G Physical Downlink Shared Channel (PDSCH) Transmission chain.

3.1 Input Parameters

A simulator for 5G must be able to work in the vast set of possible system configurations. It therefore has many input parameters. Some of the most important:

- **System Bandwidth** [MHz]
- **Signal to Noise plus Interference Ratio (SINR)** [dB]
- **Physical Cell Identity** [0,1,2...,1007] $N_{ID}^{cell} = 3N_{ID}^{(1)} + N_{ID}^{(2)}$

- **MIMO configuration** Number of TX antennas and number of RX antennas
- **CP Type** ['Normal', 'Extended']
- **Numerology μ** From which depends the SCS and the slot duration
- **Carrier Frequency f_c** [GHz]
- **SSB burst repetition period** [5 10, 20, 40, 80, 160] [ms]
- **Enable SSB soft combination** at the UE receiver ['OFF', 'ON']
- **SSB frequency position** for simplicity SSB frequency position is centered on the carrier (as for LTE)
- **Generation of the beamforming vectors** for Beam Sweeping
- **Selection of propagation Channel Model** for example simple AWGN channel or more complex fading channel
- **Mobile speed and Doppler spread**

An important design choice is that the simulator works on a slot basis: it simulates the transmission and reception of a single slot, and proceeds to the next one, iteratively.

3.2 Transmission Chain Modules

TX - (Data or Control information) generation and modulation The data to be carried into a certain channel are generated and processed. In this particular version of the simulator, the interested channel is PBCH, which creation requires all the steps explained in the previous chapter: MIB Generation, CRC insertion, Polar encoding, Rate matching, Interleaving and Bit scrambling. The PBCH is then subjected to a QPSK modulation (2 bits per symbol). Other channels could be chosen, as the Physical Downlink Control Channel (PDCCH), depending on the interested test.

TX - Subcarrier mapping The DMRS are calculated on the PBCH and input parameters. PSS and SSS signals are generated from the N_{ID}^{cell} , with a BPSK modulation (1 bit per symbol). The SSB structure can then be defined, considering parameters as the OFDM symbol and slot indexes, and SSB periodicity. PSS, SSS and PBCH are placed in their respective symbol indexes, with DMRS location scheme within PBCH symbols.

Not only the SSB is placed inside the resource grid. To make the system more realistic, there is the insertion of a PDSCH, randomly generated. Within the same OFDM symbol where SSB is transmitted, PDSCH is mapped in the subcarriers surrounding it, otherwise it occupies all the resource elements available.

The SSB burst can be transmitted only in the first (or in the last) half frame, and

then only depending on its periodicity. Thus strict controls are made on the mapping, counting the relative slot number.

TX - Multi-Antenna processing A codebook (3GPP) contains the possible beamforming vectors, based on DFT vectors. Beams for SSB are selected from 8 orthogonal beams in azimuth covering the sector, in the broadside direction in elevation and they have polarizations in phase. The scenario considered is a single panel antennas with cross-polarized elements, where the user is located in the front of the antenna: Azimuth angles of Departure (AoD) = 0° , and Zenith angles of Departure (ZoD) = 90° (figure 3.2).

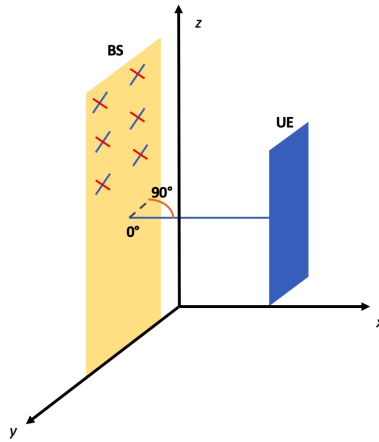


Figure 3.2: representation of the direction of the antennas w.r.t. the RX device.

For PDSCH the beamforming vector is randomly selected.

TX - OFDM signal generation The OFDM modulation is performed. One of the big advantages of OFDM is the quite simple implementation through the IFFT operation (example in figure 3.3). Before the IFFT, an ifftshift must be applied, to properly mirror the spectrum in the positive frequencies domain.

The sampling frequency determines the size of the IFFT, so the number of samples for each OFDM symbol. At this point the Cyclic prefix is inserted at the beginning of each OFDM symbol, with a duration chosen between "normal" or "extended".

TX - Transmitter Front-End An oversampling step increases the number of samples for each bit, by a certain factor. This increases the required sampling frequency, but some techniques can be implemented at the receiver to improve the reception thanks to this larger amount of samples (for example with interpolation). The overall signal is then filtered to keep the signal spectrum only within the available band, and to limit interference with the adjacent ones.

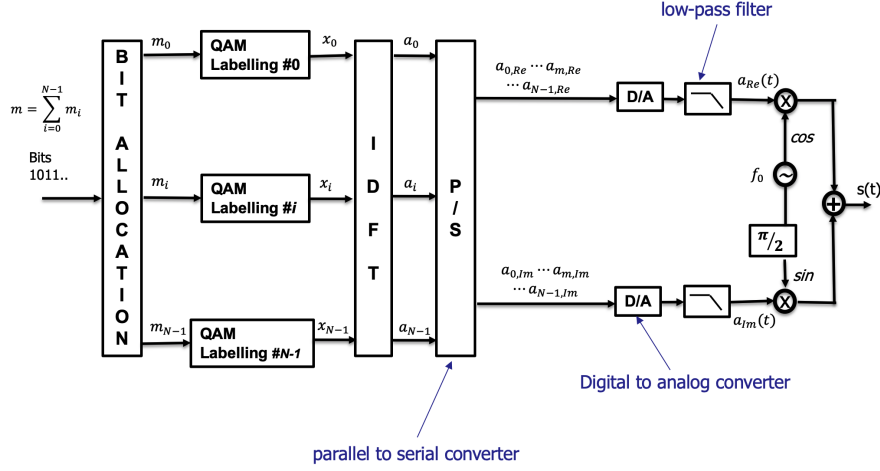


Figure 3.3: A block-scheme representation of an OFDM modulator.

Channel Model The channel model characterizes the signal propagation behaviour. There are many different kind of channel model, which each trying to better fit a particular environment. For example, in a very populated city the signal experiences multipath, given the presence of many buildings and the often absence of LOS link (NLOS). On the other side, rural areas probably have less obstacles, but a poor scattering environment could compromise the MIMO implementation.

The selection of the suitable channel model is then essential to obtain meaningful results, relative to the real scenario one is trying to simulate. In addition of the simple Additive White Gaussian Noise (AWGN) channel, the main options are simulations via Tapped Delay Line (TDL) and Clustered Delay Line (CDL). While the first is usually represented as a FIR filter with given channel coefficients within its taps, the second organizes the channel reflections in clusters. In the CDL model the antenna correlation depends on the array geometry and channel spread behaviours, allowing a better representation of beamforming because the direction of the signal in the space is modelled.

"Three CDL models, namely CDL-A, CDL-B and CDL-C are constructed to represent three different channel profiles for NLOS while CDL-D and CDL-E are constructed for LOS" and "Three TDL models, namely TDL-A, TDL-B and TDL-C, are constructed to represent three different channel profiles for NLOS while TDL-D and TDL-E are constructed for LOS" [27].

RX - Front-End The Front-End of the receiver is simulated through a filtering step, to isolate the interested bandwidth from noise, followed by a downsampler set depending on the upsampling factor inserted by the transmitter.

Before processing the downsampled signal, it is copied inside a circular buffer. It is not a realistic solution but useful in this software environment. A version of the signal is available for each RX antenna.

RX - OFDM demodulation The OFDM demodulation is the symmetric version of the modulation at the RX: it firstly removes the Cyclic Prefix, and then performs the FFT, which bring the signal from the time domain back to the frequency domain.

RX - DMRS pilot compensation and Channel estimation for PBCH based on DMRS When an SSB is transmitted inside the slot, this module compensate the DMRS pilot symbols with the product of a local replica of the conjugated pilot sequence (assumed known).

The values inside the DMRS positions can thus be used to estimate the channel coefficients. In general a greater number of pilot symbols allows a better channel estimation, but this would increase the overhead (i.e. decrease the data rate). Since each of them is related only to a certain time-frequency pair, an interpolation along both frequency and time is necessary to estimate the channel coefficients in the overall resource grid: the channel response can change both for different subcarriers and for different OFDM symbols.

There exist many interpolation techniques, with different performance but also complexity. Optimal techniques, like Discrete Wiener Interpolation, are usually not feasible solutions, but simpler techniques, like linear or cubic interpolation, can be used.

RX - Subcarrier demapping Symmetric operation w.r.t. the subcarrier mapping: the input signal is divided into each signal and channel composing it, by mean of Look Up Tables (LUTs). This procedure requires a precise resource grid alignment.

RX - Multi antenna demodulation for PBCH In this module the different sequences processed for each RX antenna are now combined to recover a single sequence. The SSB is transmitted in a single stream of data, so in case of PBCH recovery only one sequence will be found at the output.

In case of other channels and/or MIMO configurations advanced space-time equalization algorithm are needed to separate the flows.

PBCH processing A set of operations are required to translate the received sequence to the transmitted data, which accuracy affects the amount of errors.

Symbol to bit demapping exploits a soft demodulator, which receives the symbols and their constellation as input, returning soft bits. It is based on the distance of each symbol from that of the reference constellation, on the real and imaginary axes. It follows the symmetric operation of the TX on the PBCH as bit descrambling and Polar decoding.

The simulator provides an option to apply the soft combination, a function that allows to combine different SSBs to mitigate the effect of the channel and therefore reduce the probability of error.

PBCH performance evaluation Finally, the results of PBCH transmission and reception is evaluated by comparing the decoded bits with the actual transmitted ones,

giving as outputs three different performance indicators: RAW Bit Error Rate (BER), from the bits prior to the Polar Decoding, Decoded BER, after the polar Decoding, which should mitigate the channel effect, and the BLock Error Rate (BLER), which computes the errors over an entire block basis, instead of single bits.

Chapter 4

Algorithms and simulation results on Primary Synchronization Signal (PSS) detection

In this chapter the realization of the PSS detector will be discussed, the new functions added to the Link Level simulator described, and its behaviour analysed.

4.1 Detection method

In [28] three different PSS detection methods have been studied, one exploiting autocorrelation and two cross correlation. Their results depended on parameters such as Signal-to-Interference-plus-Noise-Ratio (SINR), Carrier frequency (f_c) and Carrier Frequency Offset (CFO or Δf_c). After analysing those results, and looking at results for a f_c close to our case, the more robust one appears to be "Cross-Correlation Based PSS Detection Before FO Estimation and Compensation", the one chosen to implement.

Before performing synchronization, no information is available on the transmitter, so the PSS detection must be performed by the UE (receiver side) in time domain, before applying the FFT to the input signal.

The first step consists on computing the cross correlation between the received signal and a local replica of the PSS sequence. We will obtain a correlation value for each possible delay and for each of the three possible PSS sequences. The parameter timing $\hat{\mu}_t$ and the actual PSS sequence \hat{l} (one out of three) can be found by looking at the arguments giving the maximum correlation value:

$$(\hat{\mu}_t, \hat{l}) = \arg \max_{\mu_t, l} \left| \sum_{n=0}^{N_{FFT}-1} r(n + \mu_t) \cdot \hat{d}_{PSS}^{(l)}(n)^* \right|^2$$

By using estimated received timing $\hat{\mu}_t$ and sequence \hat{l} of the PSS, we compute the partial correlation between the received PSS signal and PSS sequence replica over the former and latter $N_{FFT}/2$ sample durations of the PSS.

$$C_0 = \sum_{n=0}^{N_{FFT}/2-1} r(n + \hat{\mu}_t) \cdot \hat{d}_{PSS}^{(\hat{l})}(n)^*$$

$$C_1 = \sum_{n=0}^{N_{FFT}/2-1} r(n + N_{FFT}/2 + \hat{\mu}_t) \cdot \hat{d}_{PSS}^{(\hat{l})}(n)^*$$

Based on these partial correlations, the phase variation $\Delta\hat{\theta}$ due to the frequency offset over $N_{FFT}/2$ sample duration is estimated as:

$$\Delta\hat{\theta} = \arg \left(\frac{Im[C_1 \cdot C_0^*]}{Re[C_1 \cdot C_0^*]} \right)$$

From the estimate of $\Delta\hat{\theta}$, the fractional frequency offset is estimated as:

$$\Delta\tilde{f} = \Delta\hat{\theta} \cdot f_s / \pi N_{FFT}$$

Since $\Delta\hat{\theta}$ is periodic, also it is $\Delta\tilde{f}$, allowing us to estimate Δf_c in a range of $\pm\Delta f_{subsp}$ (see [28]).

4.2 PSS detection performance

4.3 System parameters

The first goal in the synchronization process is the detection of the PSS transmitted by the BS.

The interested system is characterized by the analysis of a received signal on a slot basis, i.e. at each iteration one slot is buffered and then processed at the receiver side.

Main parameters are:

- Carrier frequency $f_c = 3.6$ GHz
- System configuration = SISO
- Numerology $\mu = 1$
- Subcarrier spacing $\Delta f_{subsp} = 15 \text{ kHz} \cdot 2^\mu = 30 \text{ kHz}$
- Slot or Transmission Time Interval $TTI = 1 \text{ ms}/2^\mu = 0.5 \text{ ms}$

- Signal bandwidth $B = 80$ MHz
- Sampling frequency $f_s = 122.8$ MHz
- Up sampling factor $up_factor = 4$
- Channel model = Additive White Gaussian Channel (AWGN)

The SSB burst is composed by 8 SSBs, transmitted every 20 ms, and lies in the first half of the frame (i.e. during first 10 ms). More precisely, these 8 SSBs are transmitted during the first 4 slots of the frame, leading to 2 SSBs per slot, organized as in figure 4.1: first SSB occupies OFDM symbols from #2 to #5, and second SSB occupies OFDM symbols from #8 to #11.

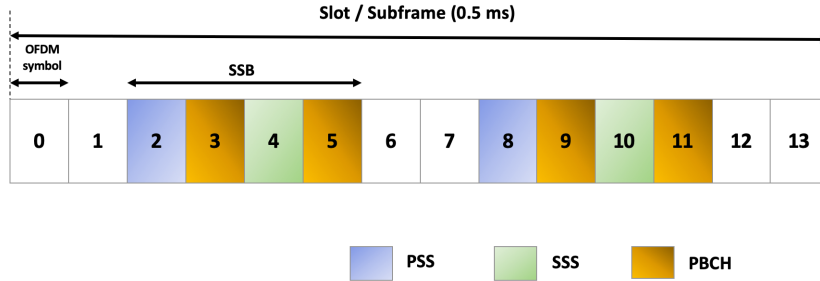


Figure 4.1: Subframe organization.

We will consider each SSB separately, without any sort of time accumulation (i.e. without coherent or non-coherent sum). This solution is chosen in order to consider further implementations with beam sweeping, so each SSB could belong to a different beam aligned in a different direction. Nevertheless, thanks to receiver diversity, space accumulation could improve the performance, but we still do not consider it, obtaining a sort of lower bound on the performances.

4.4 Implementation of Cross Correlation

A key point is the translation of the mathematical expressions defined for the correlation into suitable solutions for the actual implementation.

To compute the cross correlation between received signal and local replica, a FIR matched filter is used (example in figure 4.2), represented by the expression:

$$\rho[n] = \sum_{k=0}^{N-1} b[k] \cdot r[n - k]$$

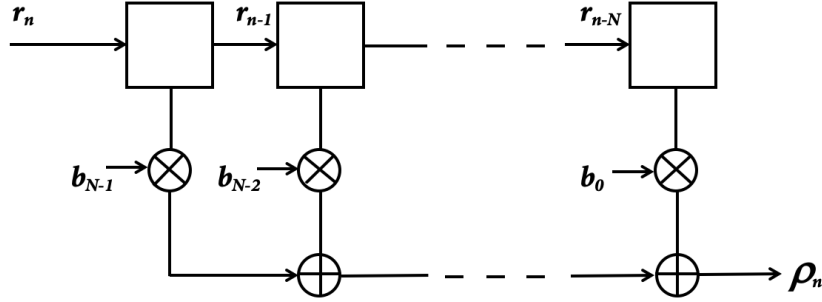


Figure 4.2: Example of FIR matched filter.

The quantity of filter coefficients (also called taps) should be far below the number of FFT samples per symbol, which are in this case 4096. In fact, the real implementation imposes some limits on the filter length, due to complexity issues, which can be respected with only 256 (or, alternatively, 512) taps. A downsampler is then required to pass from the upsampled received signal to the required sequence characterized by 256 samples per OFDM symbol, with a factor:

$$\text{Downsampling_factor} = \text{up_factor} \cdot 16 = 4 \cdot 16 = 64$$

Where 16 is given from $\frac{4096}{256}$.

The actual minimum number of FIR coefficients comes from the SSB definition: an SSB occupies a bandwidth of $30 \text{ kHz} \cdot 240 \text{ subcarriers} = 7.2 \text{ MHz}$, so 256 is the closest power of 2 above it, corresponding to a bandwidth of $30 \text{ kHz} \cdot 256 \text{ subcarriers} = 7.68 \text{ MHz}$. From the point of view of the local replica of the PSS, 256 is practically the double of its length (which is 127). Thus, before applying the IFFT also to the local replica (in order to switch in time domain), a zero padding at both ends is required to get a sequence of 256 values.

Before downsampling the input signal, a proper Anti-Aliasing (AA) Low Pass (LP) Filter must be applied, in order to remove (or at least reduce) the noise components, included the other channels transmitted by the BS. The implemented solution is an AA LP filter with Kaiser-Bessel Window¹. It is an approximation of the DPSS (Discrete Prolate Spheroidal Sequence) Window, which tries to maximize the energy concentration in the main lobe, but which would be too difficult to compute.

Applying a standard Lp filter without a correct interpolation would lead to not respect the Nyquist ISI criterion, losing the good correlation properties of the PSS sequence.

The need of downsampling is a non ideality and could lead to performance degradation. An evaluation of this effect can be performed, comparing the correlation power

¹A window is a mathematical function zero-valued outside a closed interval, usually symmetric with a centred maximum.

measured with and without the downsampler. We define a particular measure called Quality Indicator (QI), which represents a sort of SNR calculated over the correlation values. It is the ratio of the correlation power maximum, over the noise variance. With noise we are referring to every value outside the correlation peak.

The upper bound is the ideal case without downsampling and when nothing is transmitted except for the PSS, so the noise in the correlation can be generated only by the noise introduced from the channel and not by other subcarriers.

The maximum of the correlation power could be not the one of the PSS detection, so an approximate lower bound for signalling values of QI for an unreliable detection is defined: if QI is lower than this bound, probably the detection will not be successful.

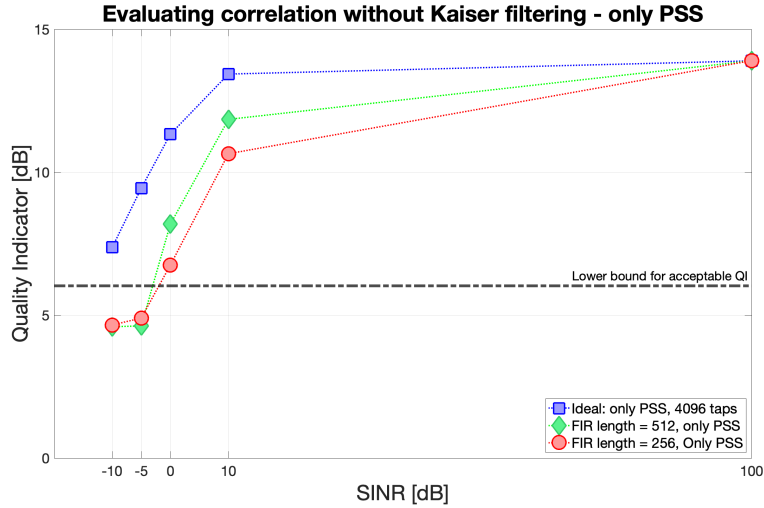


Figure 4.3: Quality indicator in case when no channels or signals are transmitted, except for PSS.

In figure 4.3 the huge degradation effect caused by a downsampling missing the AA filter is shown, even if only the PSS sequence is transmitted.

Fortunately, as shown in figure 4.4, it appears that, in the most interesting range of SINR values, the solutions adopting the AA filter does not behave too much worse than the ideal one, which is also a very utopian upper limit. Moreover, in low SINR conditions, the predominant effect is the channel noise, rather than the presence of other channels.

The last plot, figure 4.5, is very interesting: it shows how the introduction of the AA filter can almost make us neglect the worsening produced by the downsampler.

The insertion of a block in the simulator for the PSS detection updates the overall transmission chain, as shown in figure 4.6), and the PSS detector main components are zoomed in figure 4.7).

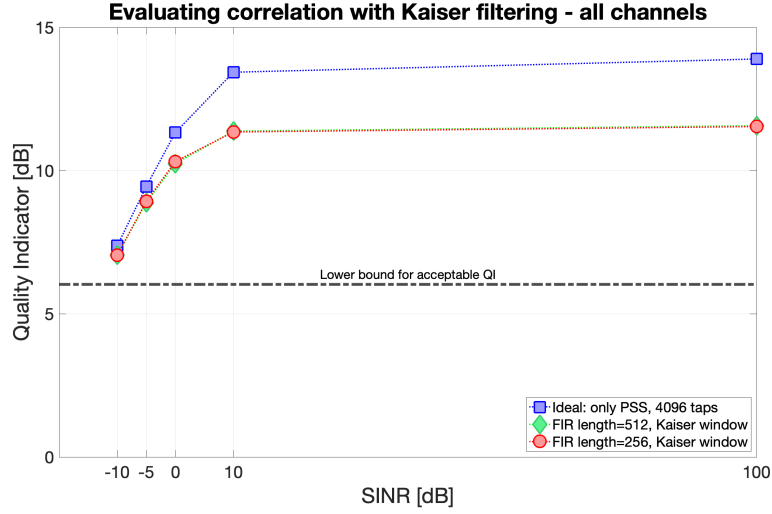


Figure 4.4: Quality indicator in case when all channels and signals are transmitted, using Kaiser filtering, w.r.t. an ideal case.

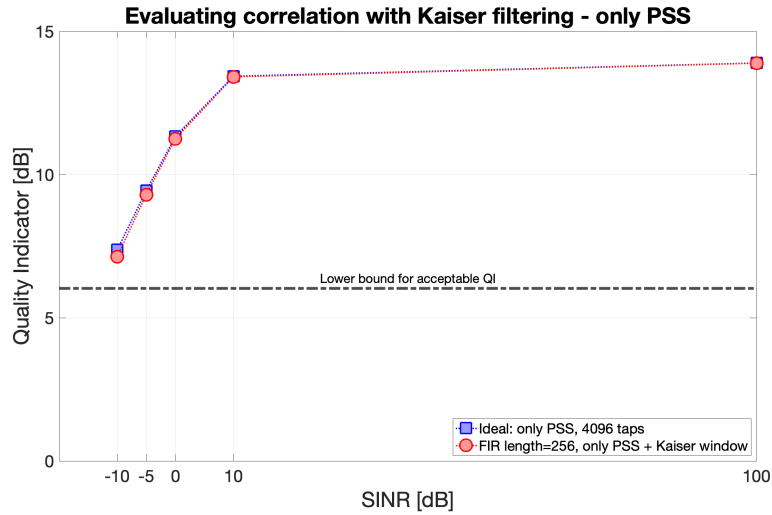


Figure 4.5: Quality indicator in case when no channels or signals are transmitted, except for PSS, using also Kaiser filtering.

4.4.1 Integer Frequency Offset Estimation

Previously, the fractional frequency estimation technique has been presented. In case of $|CFO| > 30$ kHz, estimating the FFO is not enough, and we should also consider the Integer Frequency Offset (IFO, or G):

$$FO = FFO + IFO \cdot \Delta f_{subsp}$$

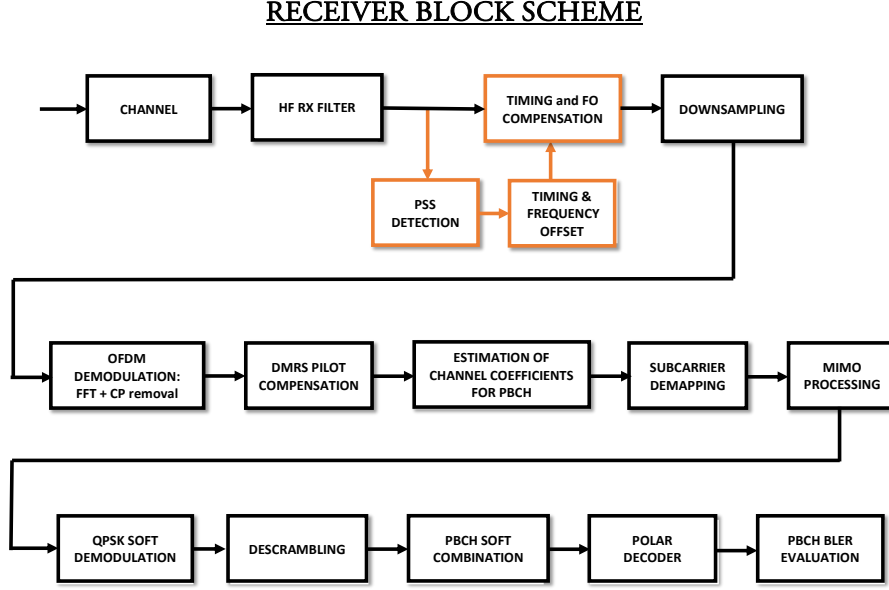


Figure 4.6: Simulator block scheme with PSS detection.

The correlation function gives a simple way to estimate this IFO, by correlating the local replica of the PSS sequence with the received signal compensated for the timing (aligned at the beginning of the PSS). Received signal is also compensated for a set of different FO values, corresponding to the FFO plus multiples of Δf_{subsp} , both positive and negative.

The new versions of the received signal become:

$$\tilde{r}_G(n) = r(n) \cdot \exp[-jn2\pi(\Delta\tilde{f} + G \cdot \Delta f_{subsp})]$$

IFO is then found through the value maximizing the correlation:

$$(\hat{G}) = \arg \max_G \sum_{G=-m}^m \left| \sum_{n=0}^{N_{FFT}-1} \tilde{r}_G(n + \hat{\mu}_t) \cdot \hat{d}_{PSS}^{(l)}(n)^* \right|^2$$

The complexity of this operation is quite low, depending on the amount of G values we want to search for, but two aspects make its implementation useless:

- **Expected CFO.** Looking at the *3gpp* requirements: "*The UE modulated carrier frequency shall be accurate to within ± 0.1 PPM observed over a period of 1 ms compared to the carrier frequency received from the NR Node B*"[29]. We observe how an accuracy of 0.1 PPM of the Oscillator could never produce a CFO greater than the subcarrier spacing. In table 4.1 some possible values for the CFO at different f_c are reported.

PSS DETECTION

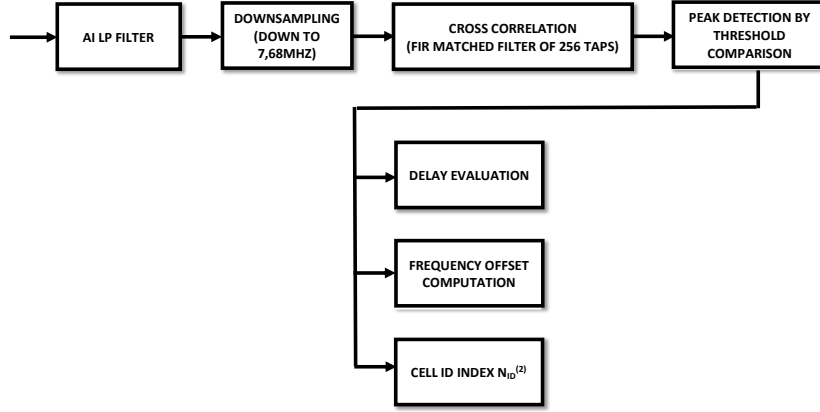


Figure 4.7: PSS detector functions.

f_c GHz	$\varepsilon = 0.1$ ppm kHz	$\varepsilon = 0.5$ ppm kHz	$\varepsilon = 1$ ppm kHz
1.8	0,18	0,90	0,18
3.6	0,36	1,8	3,6
6	0,60	3	6
36	3,6	18	36
60	6	30	60

Table 4.1: Values of CFO for different possible oscillators' accuracies.

Large CFOs can be found only in case of high f_c , but we have also to consider that usually higher numerology μ (and so subcarrier spacing) is adopted in such systems. We should also consider the frequency misalignment caused by Doppler Shift, but we are still inside a safe region. Considering the limited size of 5G cells, a reasonable speed a UE can experience is $v_0 = 50$ Km/h ≈ 14 m/s, producing a Doppler frequency shift of:

$$\Delta f'_D = \frac{v_0}{c} \cdot f_c = \frac{14 \text{ m/s}}{3 \cdot 10^8} \cdot 3,6 \cdot 10^9 = 168 \text{ Hz}$$

Value of $\Delta f'_D$ in this order of magnitude should not put in trouble our system.

An interesting study case is the 5G implementation with LEO² satellites, where involved speeds can be very large and so causing relevant Doppler shifts. Probably different techniques should be studied in such conditions, but this is not our goal.

- **Detector limitations.** As it will be shown in next sections, with the implemented technique of cross correlation after FO estimation and compensation, the correlation peak completely disappears for CFOs bigger or smaller than approximately ± 23 kHz.

This let us easily ignore the IFO estimation, even if a Matlab function was still implemented and tested.

As a final consideration, scenarios where IFO estimation becomes mandatory, different techniques should be implemented, for example estimating and compensating CFO before searching for the timing, by mean of the autocorrelation of the PSS (or of the CP).

4.5 Methodology applied for performance evaluation

As a first thought, to evaluate the detector behaviour, we could adopt a Binary Hypothesis Testing, where the null hypothesis H_0 represents the case of slot without PSS, and the alternative hypothesis H_1 otherwise corresponds to the presence of PSS. Studying a little deeper all the possible outcomes, it turned out that this solution does not completely fit the system. But we still need a threshold in order to decide whenever a correlation peak is supposed to be found.

To evaluate the performance of the detection procedure, the following hypothesis are considered:

Slot without SSB The resulting events can be:

- **Correct non-detection**, when noise is lower than the threshold. The UE correctly detects the lack of the PSS;
- **False alarm**, when at least one noise sample is above threshold. This is a particularly harmful outcome, since it can lead to set wrong synchronization parameters or to waste time trying to attach to a BS that does not actually exist.

Slot with SSB This case is a little bit more tricky than the previous. The resulting events can be:

- **Correct detection**, when correlation peak is above the threshold and above any other noise value. The UE correctly detects the presence of the PSS;

²Low Earth Orbit

- **Missed detection**, when PSS correlation peak is lower than the threshold or than the noise;
- **False alarm**, when noise is higher than both the threshold and the correlation peak.

False alarm outcomes are possible in both cases, thus preventing the definition of Receiver Operating Characteristic (ROC) curves: especially for low values of SINR, the probability of correct detection may never reach 1, whatever the threshold. The chosen representation is to plot the probability of missed detection and false alarm as a function of the threshold.

4.5.1 Threshold tuning

One key parameter in order to get reasonable results in the detection process is the threshold, i.e. the value that has to be compared with the correlation function in order to detect a candidate correlation peak. If it is set too low it could lead to high probability of false alarm, while if it is set too high could produce high number of missed detections.

The threshold expression thus takes into account the noise, estimated over the samples coming from the cross correlation computation. It also depends on a scalar factor (T_{factor}), that can be tuned by studying the performance of the detection varying its amplitude.

The mathematical expression of the threshold V_t is defined as:

$$V_t = \sigma \cdot \sqrt{-2 \cdot \ln(T_{factor})} \quad (4.1)$$

Looking at the following results will help us to correctly set a proper threshold, obtaining the right trade off between correct detection and false alarm. An acceptable design solution should be: probability of false alarm = 0.01, probability of correct detection = 0.99. Figure 4.8 is an example of the PSS detector cross correlation output with the threshold comparison.

4.6 Detector performance in low SINR conditions

In this section the performance of the detector are tested in particularly low SINR conditions. The interested indicators are the probability of missed detection and the probability of false alarm, in function of different values of CFO. We are considering pretty high values of CFO, temporarily neglecting our consideration on its actual expected amplitude. This decision has been taken in order to test the limits of this technique, and to report data open to different requirements or conditions.

Different scenarios have been simulated, and for each of them a set of data has been collected. The results are reported below:

- SINR = -6 dB (figure 4.9). With no frequency misalignment the detector works smoothly, and no PSS are missed. Even with CFO it almost never makes mistakes.

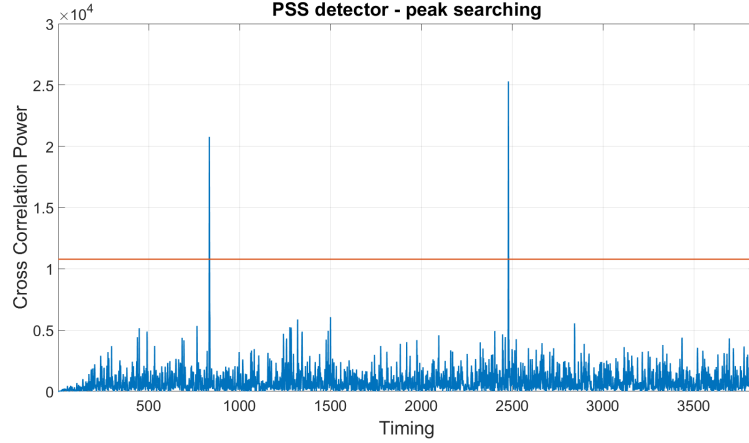


Figure 4.8: Example of the PSS detector output with the threshold comparison.

As expected, when increasing the frequency offset also the probability of missed detection increases, while false alarm keeps almost the same behaviour.

- SINR = -8 dB (figure 4.10). Missed detection curves shows up. Anyway, with acceptable values of false alarm, the detector still satisfy the requirements, even for higher CFO.
- SINR = -10 dB (figure 4.11). Performance degrades a lot. Only with none or little Frequency Offset the detection of the PSS could be performed, and still with a correct detection probability that hardly exceeds 0.95, except accepting higher values of false alarm.
- SINR = -12 dB (figure 4.12). The detector acts very poorly. It can not be used with this noise level.

The previous analysis confirmed our expectations: the detector works well even up to certain particularly low levels of SINR, but we cannot expect good results going down beyond -8 dB.

This is not a big problem since, with such low SINRs levels, an acceptable communication between UE and BS could not anyway be performed; stressing out the presence of a single receiving antenna.

In all cases we can observe a sort of constant relation between the threshold factor and the probability of false alarm, which behaviours look pretty similar. This means that, fixed a certain threshold, we can expect almost the same amount of false positives occurrences in different conditions, while the number of correct detections can still change.

In figure 4.13 only the results with no frequency deviation have been compared, for the three different SINR levels ($[-6; -8; -10]$ dB). One straight line, corresponding to $prob\ false\ alarm = prob\ missed\ detection = 10^{-2}$, divide the figure in two parts: looking at the lower one, we can choose an appropriate threshold factor, to balance between

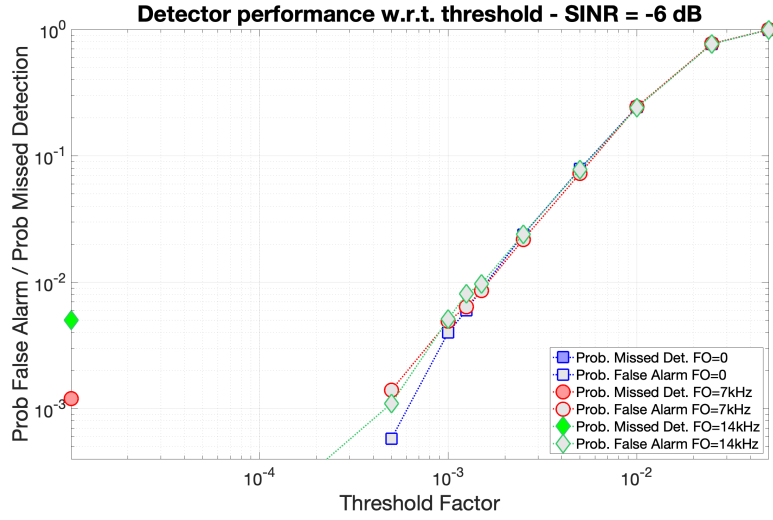


Figure 4.9: PSS detection performance with SINR = -6 dB.

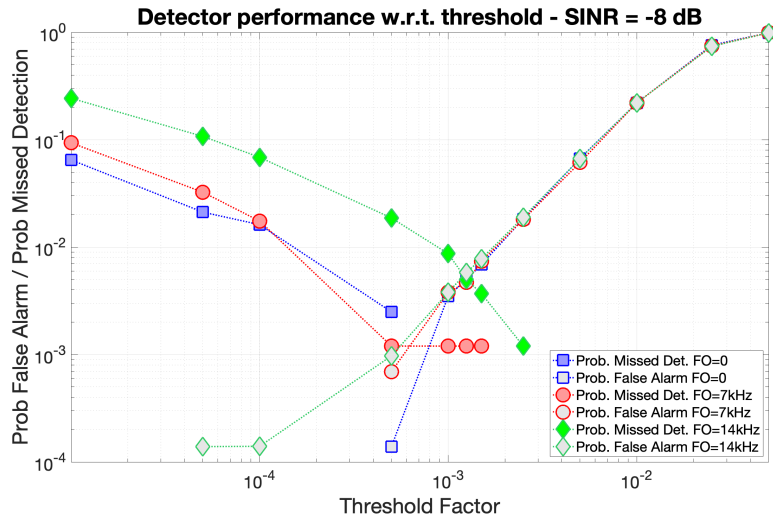


Figure 4.10: PSS detection performance with SINR = -8 dB.

probability of missed detection and false alarm. The critical working point is -6 dB, so fortunately there is a wide range of candidates.

4.7 Detector performance in CFO estimation

As already described before, CFO can largely impact the transmission, so its estimation must be as accurate as possible.

In order to evaluate the goodness of the implemented technique, a certain number of tests have been performed. The goal is to relate precision and accuracy of the estimated

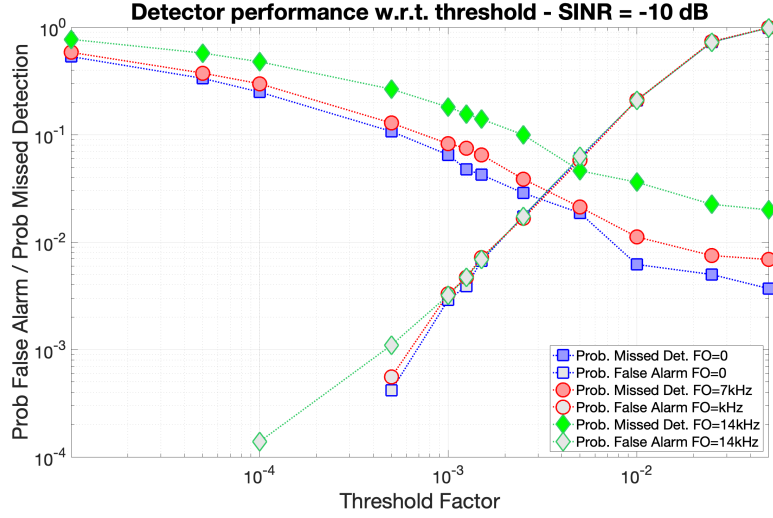


Figure 4.11: PSS detection performance with SINR = -10 dB.

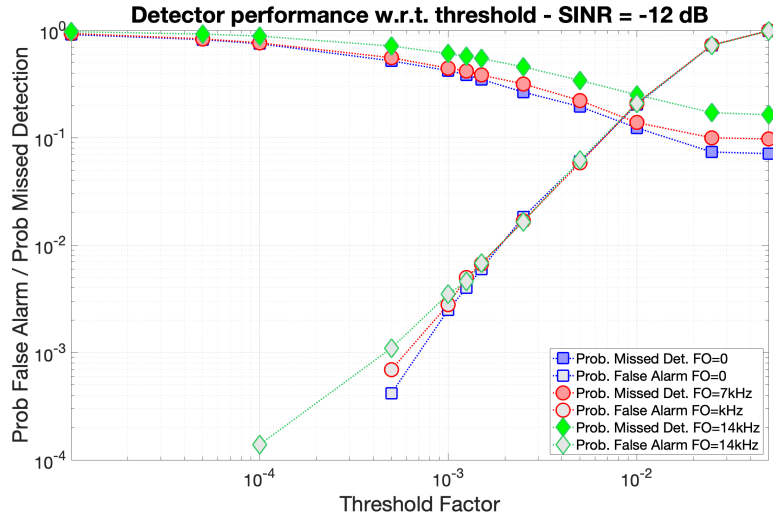


Figure 4.12: PSS detection performance with SINR = -12 dB.

FO values with two parameters, the SINR level and the actual CFO amplitude. We could expect that the estimation error is directly proportional to the nominal CFO and inversely proportional to the SINR. The quantities chosen to grade the system are the mean value (to evaluate accuracy), the standard deviation (to evaluate precision), and the Root Mean Square Error (RMSE), defined as:

$$RMSE = \sqrt{\frac{\sum_{i=1}^n (x_i - \hat{x}_i)^2}{n}}$$

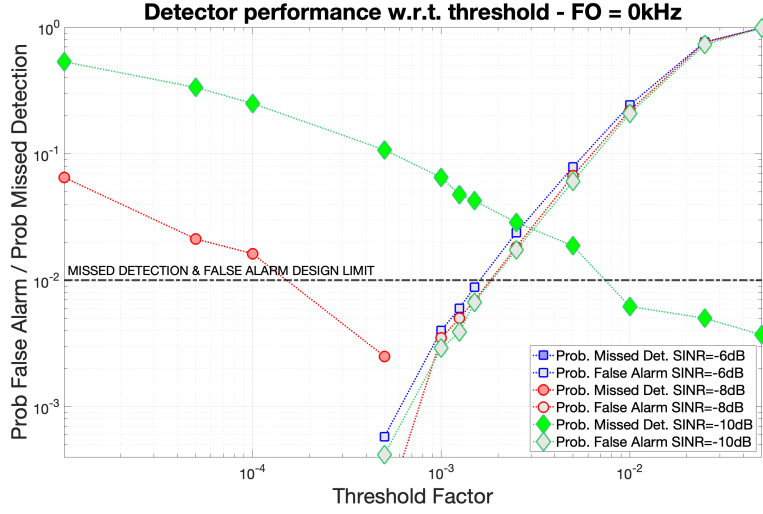


Figure 4.13: PSS detection performance with $FO = 0$ Hz.

In the following table 4.2 the results are reported:

FO kHz	SINR 10 dB			SINR 5 dB			SINR 0 dB		
	Mean kHz	Std kHz	Rmse kHz	Mean kHz	Std kHz	Rmse kHz	Mean kHz	Std kHz	Rmse kHz
0	-0.01	0.33	0.33	-0.01	0.5	0.5	-0.01	0.87	0.87
5	5	0.33	0.33	5	0.52	0.52	5.05	0.88	0.88
10	10	0.36	0.36	10	0.56	0.56	10	0.94	0.94
15	15	0.37	0.37	15	0.59	0.59	15	1	1
20	20	0.42	0.42	20	0.66	0.66	20	1.05	1.05

FO kHz	SINR -5 dB			SINR -10 dB		
	Mean kHz	Std kHz	Rmse kHz	Mean kHz	Std kHz	Rmse kHz
0	-0.02	1.5	1.5	-0.13	2.7	2.7
5	5.1	1.5	1.5	5	2.7	2.7
10	10	1.7	1.7	9.1	2.9	3
15	15	1.7	1.7	13	1.6	2.8
20	18	2.6	3.4	-	-	-

Table 4.2: Results from the frequency offset estimation over 20 SSBs.

Three plots have been generated to report the three quantities for five different SINRs: mean values in figure 4.14, standard deviations in figure 4.15 and RMSEs in figure 4.16.

Curves show how the measurement errors comply with our thoughts on the behaviour w.r.t. both SINR and CFO amplitude. The noise enhancement makes the estimator

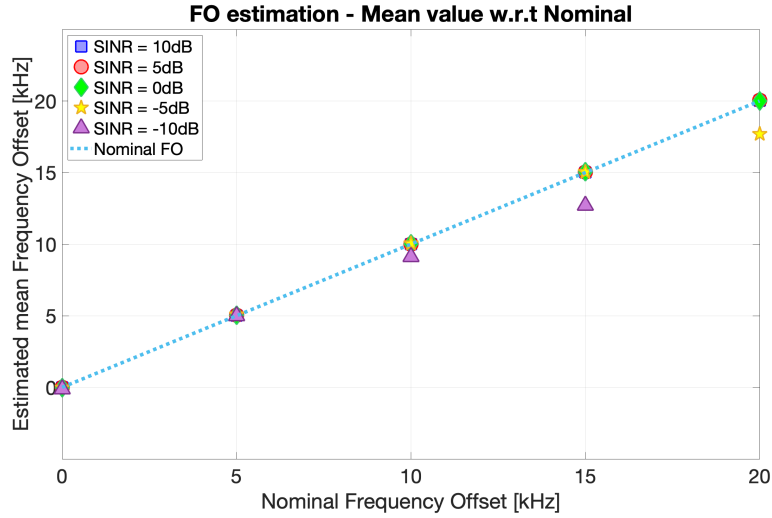


Figure 4.14: Frequency Offset measurements: mean value for different SINR levels.

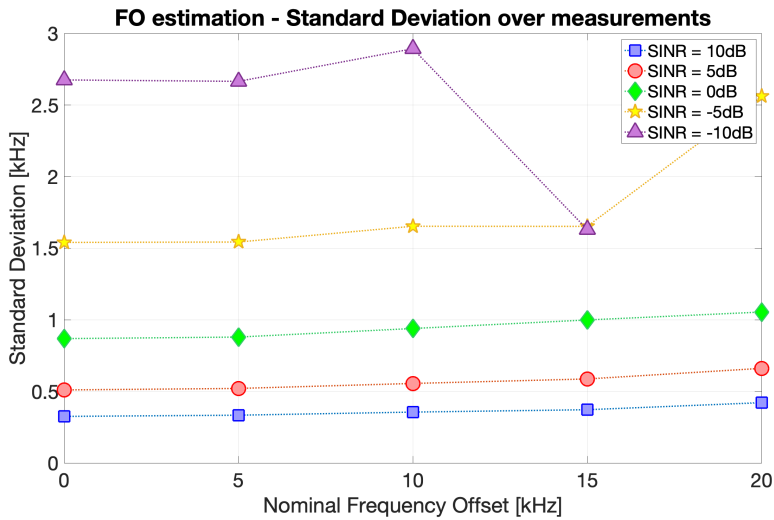


Figure 4.15: Frequency Offset measurements: standard deviation for different SINR levels.

less efficient, considering also the limited length of the filter, unable to perform a great averaging over the noisy samples. Using longer filters could produce better results, but it is not a solution often available.

This can be still seen as a good result for CFO values over than a certain level, where most of the misalignment can be corrected, but not too good for small ones, where compensating for the CFO could even lead to increase the frequency misalignment. Fortunately, small values of CFO do not represent big problems in this initial process, so we could leave the compensation of small CFO (up to 2 kHz) to finer techniques.

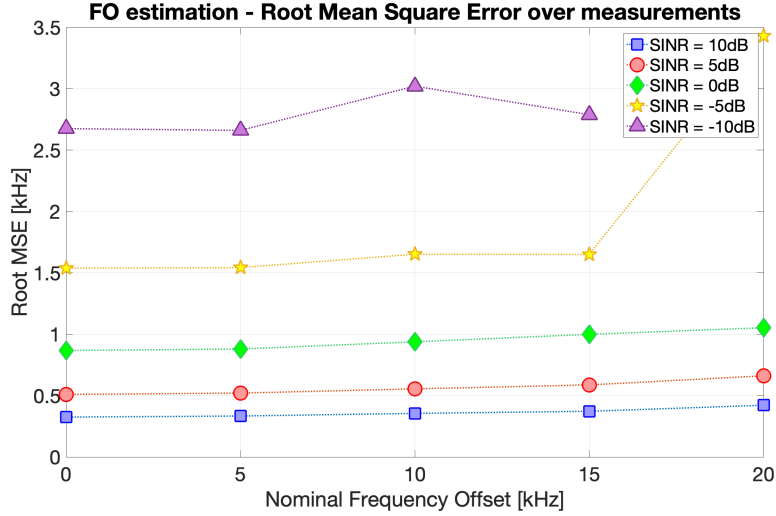


Figure 4.16: Frequency Offset measurements: root means square error for different SINR levels.

For very low value of SINR, this estimation becomes particularly unreliable, also considering that often no correlation peak is found and so no estimation can be performed. Also a CFO of 20 kHz can lead to many missed detection, so the behaviour of the estimation w.r.t. the SINR can be a little bit misleading; e.g. standard deviation for SINR of -10 dB seems the same as standard deviation for SINR of -5 dB, but from the RMSE plot we can see how the error is actually bigger.

4.8 Detector performance in the critical working point

Fixed the threshold expression, a deeper focus on the detector performance can be done. In this case a longer simulation has been run: 4000 slots have been processed, for a total amount of 800 SSBs (one SSB burst each 40 subframes). The smallest resolution for probability of missed detection is then $1,25 \cdot 10^{-3}$. The SINR is kept fixed at -6 dB, while the CFO is progressively changed. The probability of false alarm is not reported but is kept a little lower than 10^{-2} .

Figure 4.17 shows the probability of correct detection, while figure 4.18 shows the mean of estimated CFO with an interval corresponding to the standard deviation. Both figures are in function of increasing CFOs.

This additional test seems to confirm the previous observations. For small values of Frequency Offset (up to 15 kHz) the detector works as required, and this should be the case considering the *3gpp* requirements. On the other hand, CFO estimation could counteract this effect, but its usage should be studied carefully. In fact, only with a pretty large collection of estimations we could get a mean FO acceptable for the

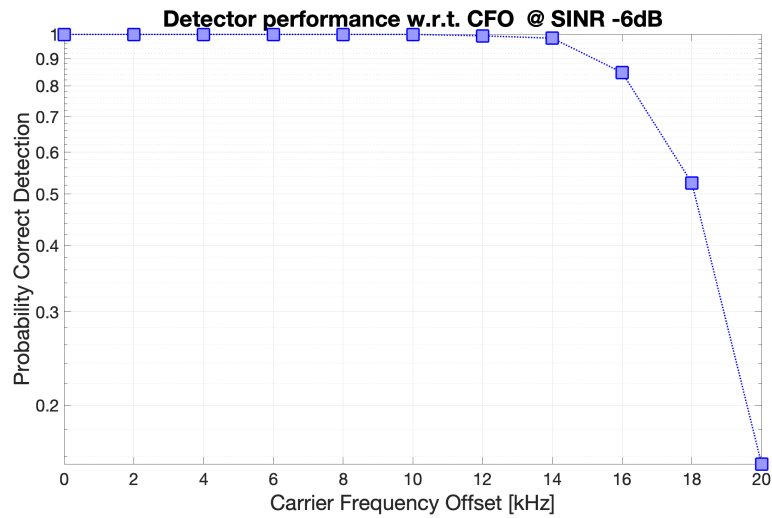


Figure 4.17: Critical working point: Behaviour of probability of correct detection w.r.t CFO.

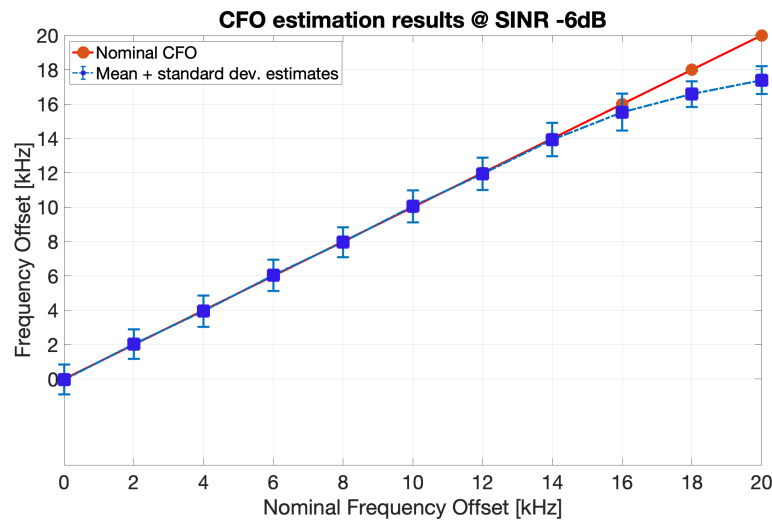


Figure 4.18: Critical working point: CFO estimated mean and standard deviation.

compensation, otherwise we should try for compensate only CFO bigger than a lower limit, that can be chosen by design (standard deviation is relatively high and it could lead to increase the misalignment).

This problem will be addressed in the next chapter.

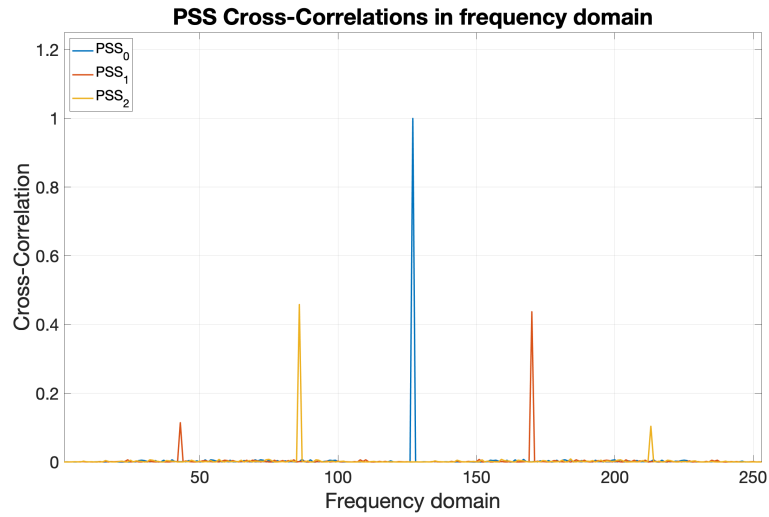
4.9 Considering the other PSS sequences

In previous tests it was considered known which of the 3 PSS sequences had been transmitted, and therefore the detection calculated the correlation with the appropriate local replica, without having to test all three possibilities. It simplified the whole procedure, also considering the good correlation properties of the m-sequences, which therefore should not affect the performance of the detector: the three PSSs are the cyclic shift of each other, so this could generate undesired correlation peaks if the matched filter would work in the frequency domain, but the IFFT applied to the signal, passing then to time domain, prevents this outcome, as shown in figure 4.19.

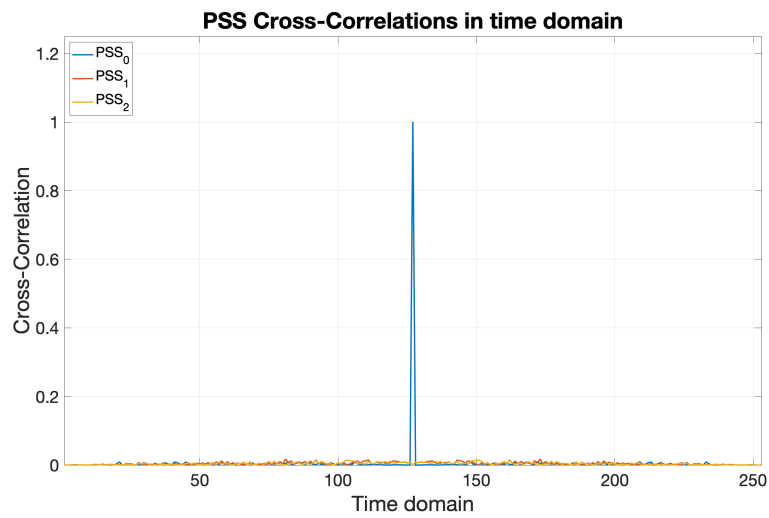
Now, wishing to deepen this aspect, an expansion of the detector is performed, considering the PSS sequence actually transmitted unknown. A suitable configuration for this purpose is shown in figure 4.20: 3 matched filters in parallel calculate the correlation of the input signal with the 3 possible PSSs, the results are then individually subjected to a threshold comparison and, if more than one peak is detected, they are compared and the maximum is chosen. This last step could be more complex in reality, since the presence of different peaks could refer to several cells, detecting more PBCH at the same time. Considering the transmission as point-to-point, it will not be studied here.

Following a procedure for measurements similar to those carried out so far, a counter is implemented to return the number of times the detector does not identify the correct sequence, or when all the peaks were below the threshold (in an entire simulator cycle, the maximum detectable PSSs are 800).

In figure 4.21 the bar plots report the results of the counting with different input parameters. As we could have expected, the good cross correlation properties allow to neglect the possibility of choosing the wrong $N_{ID}^{(2)}$ after the detection, being robust against SINR and CFO inside the reliability intervals identified from the previous graphs.



(a)



(b)

Figure 4.19: PSS m-sequence cross-correlation, among the three possible different PSSs when PSS_0 is transmitted.

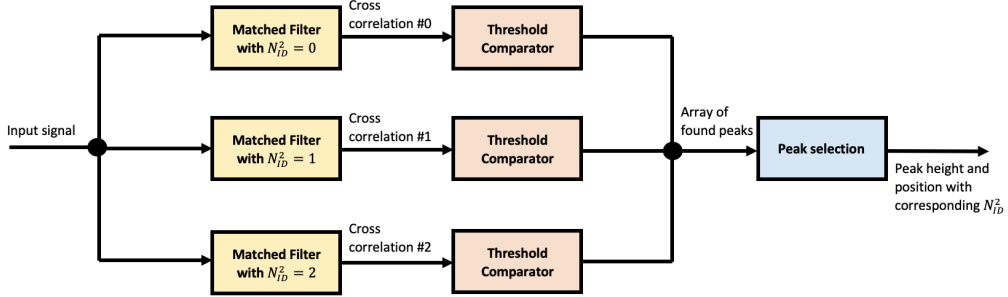


Figure 4.20: Hardware implementation for the PSS detection, considering three possible sequences.

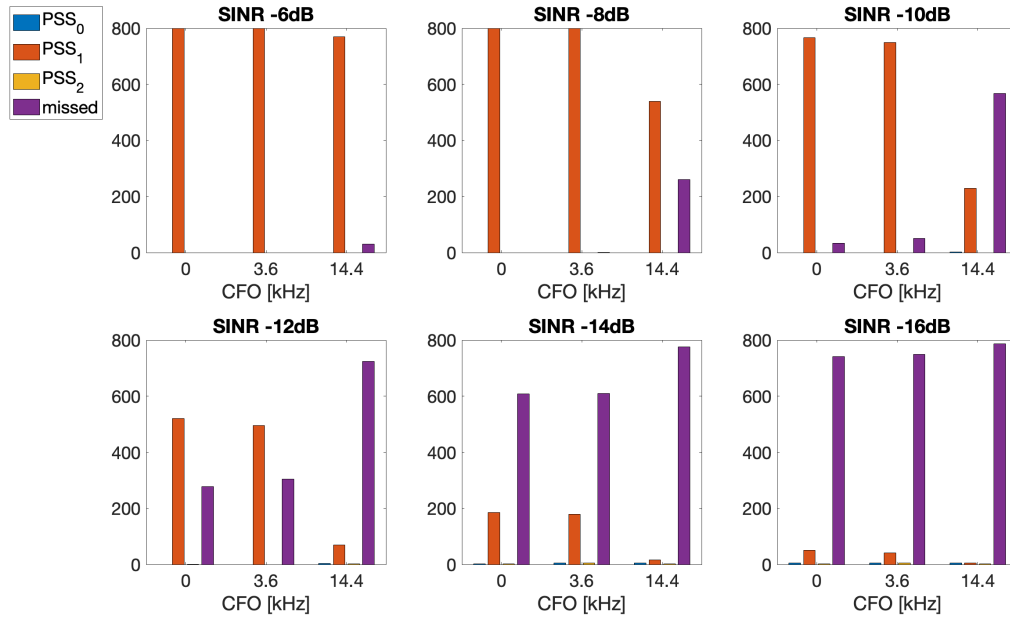


Figure 4.21: Bars counting if and which PSS sequence has been detected, in case of different SINRs and CFOs, when PSS_1 is transmitted.

Chapter 5

Physical Broadcast CHannel (PBCH) performance analysis

In this chapter the study on the synchronization procedure will be deepened by analysing how the PBCH performance varies with the insertion of the PSS detector.

New parameters will be considered to make the system more complete, such as the increase in the number of antennas at the receiver and the signal propagation delay, studying how they affect the results and adapting the PSS detector accordingly.

5.1 Frequency Offset effect on the system

Given the described pre-existing system for the PBCH processing, the goal is to analyse a more realistic scenario, as for the PSS detection part, with the frequency offset impairment.

We expect that the CFO can worsen a lot the performance, since no techniques of CFO compensation is provided within PBCH recovery. Probably, for small CFO values, the errors from the distortion of the scattering diagram can be managed by the coding technique. Anyway, also considering the possibilities of low SINR levels, its effect could completely disrupt the synchronization procedure.

In this section the CFO effect on the performance will be studied, by using the module for the CFO insertion as in the previous chapter, and then collecting the output values of BLER.

The ideal case is compared with 3 different cases of CFO, still assuming a carrier frequency $f_c = 3.6$ GHz:

- 0.5 ppm \rightarrow 1.8 kHz
- 1 ppm \rightarrow 3.6 kHz
- 2 ppm \rightarrow 7.2 kHz

As we can see in figure 5.1, for the smallest value the performance does not change excessively (approximately less than 1 dB). If we double it, the situation gets a lot worse. Finally, for the 7.2 kHz case the receiver can not even recover the PBCH at all, neither for higher SINR levels.

The experiment is then repeated for increasing values of receiving antennas: 2 in figure 5.2 and 4 in figure 5.3. Of course the system becomes more robust against SINR, with a gain of about 2 dB (shown in figure 5.4). Doubling the number of antennas, we could expect at maximum about 3 dB of gain¹ each time, but the various processing steps performed by the receiver probably do not allow the application of this simple rule of thumb. Moreover, the thermal noise of the receiver imposes a minimum amount of useful signal power to work, so the gain usually decrease with lower SINR. The behaviour of the BLER w.r.t CFO is pretty the same for each receiving antennas quantity option.

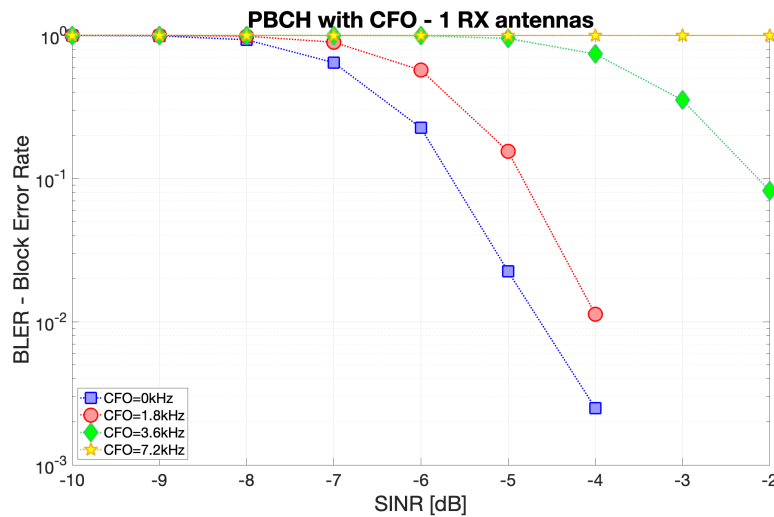


Figure 5.1: BLER for PBCH with CFO insertion, 1 RX antenna.

5.2 Compensation of CFO estimated from PSS detection step

In the previous section it became clear how CFO misalignment can't be neglected: a compensation step must be designed to provide a more reliable system.

This is the point where the module developed for the PSS detector comes to our aid. Enabling the PSS processing before PBCH operations will output a CFO estimation that can be used to compensate the interested signal. We would expect that, after got

¹Measured on the SINR for a certain target BER

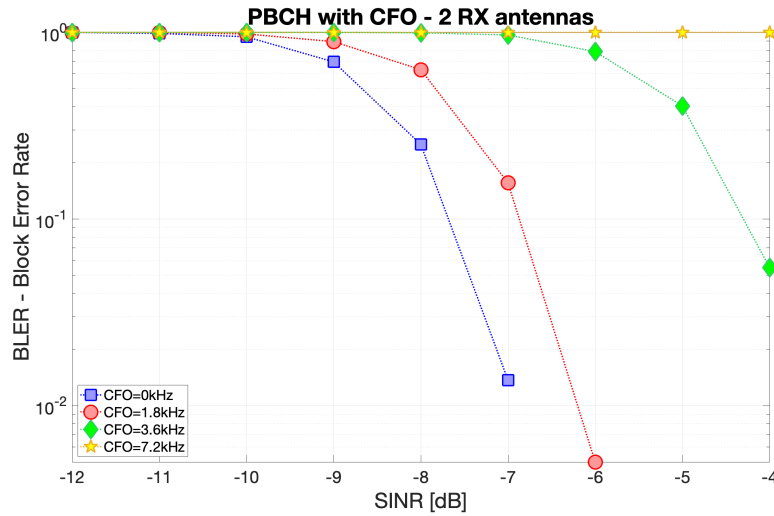


Figure 5.2: BLER for PBCH with CFO insertion, 2 RX antennas.

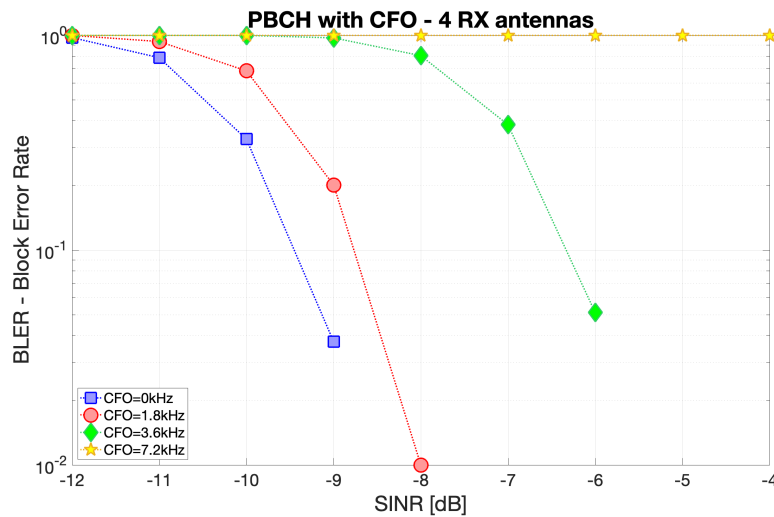


Figure 5.3: BLER for PBCH with CFO insertion, 4 RX antennas.

rid off this impairment, the performance of the system returns to be as good as the ideal initial case.

In reality, looking at the measurements on the frequency offset estimation, we see that the error of the estimation can be quite high. This means that a residual frequency offset will still be present, avoiding the system to perform as in the ideal case. We should then analyse the distance between the different BLER curves.

One new element that we have to consider here is that, in case of more than one receiving antenna, more CFO estimates are available at the same time (one for each antenna). A reasonable solution is then to exploit this set of values to perform an

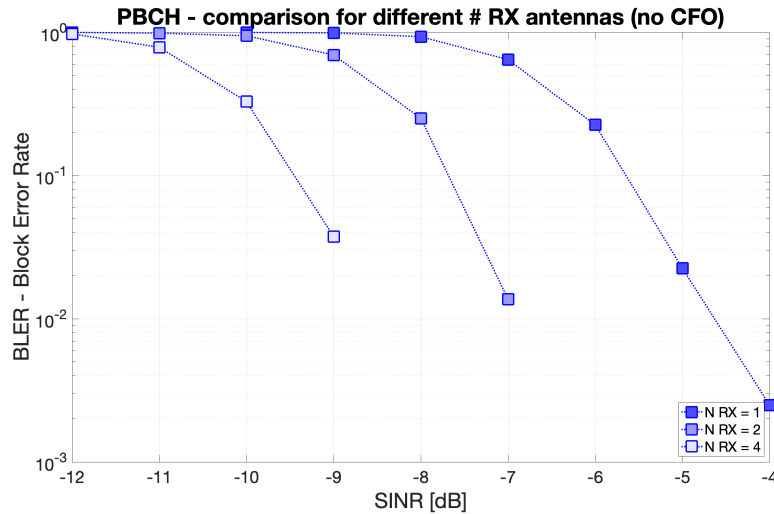


Figure 5.4: Comparison of BLER for PBCH for different number of RX antennas (no CFO).

accumulation. We average them, expecting a better frequency correction.

In figure 5.5, figure 5.6 and figure 5.7 the results are reported. For the highest values of CFO, the compensation leads to a clear improvement. The most evident example is the curve of 7.2 kHz, which is closer to the other ones, while without compensation it was impossible to recover the PBCH. For the 1.8 kHz value instead, the curves of the compensation case almost overlap, and are slightly closer to the ideal case with more antennas.

The performance is not the best we would have desired, but it could be still acceptable (losses are in the order of 1 dB) and greatly useful for high values of CFO.

5.2.1 Improving frequency offset estimation: time averaging

We now investigate if and how it is possible to get better results. One pretty easy solution is of course the averaging along time of the measured CFO values, in combination with space averaging (for many RX antennas).

Still considering an 8 beam system, we can't sum subsequent estimates, even if it would be simpler. We must sum the outcomes provided by the same beam number, which are spaced 20 ms in time (one every 40 subframes). Since this could be a problem for the synchronization duration, we set the maximum number of values up to 80 ms, i.e. 4 estimates, which also corresponds to the TTI (Transmission Time Interval) of the PBCH.

There could be different ways to combine the different outcomes. In this implementation a weighting system has been chosen, giving the bigger weight to the last estimate, and decreasing the amplitude of the weights by time order (the first one in time will have the smallest weight).

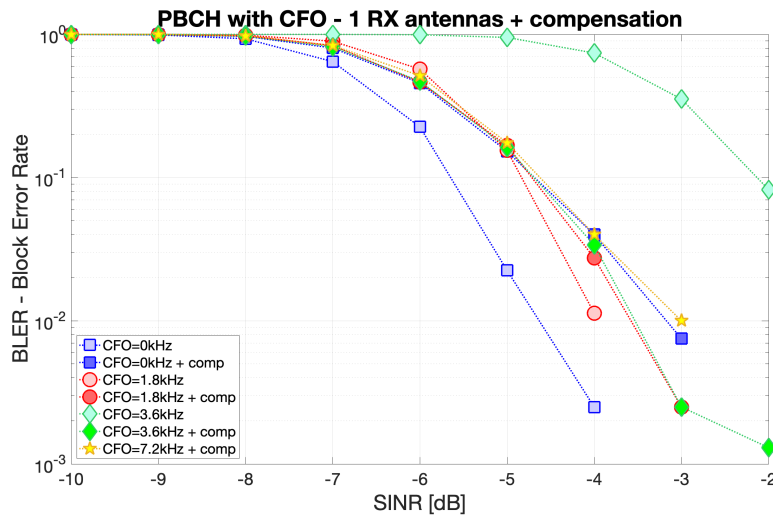


Figure 5.5: BLER for PBCH with CFO insertion and compensation, 1 RX antenna.

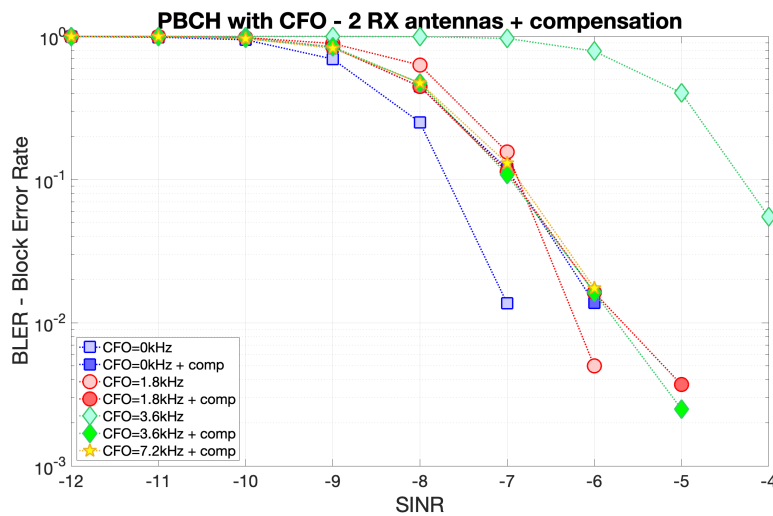


Figure 5.6: BLER for PBCH with CFO insertion and compensation, 2 RX antennas.

In figure 5.8, figure 5.9 and figure 5.10 the results are reported. Our goal of improving the previous results seems to be achieved: the curves related to the system with compensation are much closer to the ideal case. This means that, with time and (if available) space averaging, the PSS detection permits to increase the robustness of the PBCH recovery against CFO, without being a problem for very small values of this misalignment.

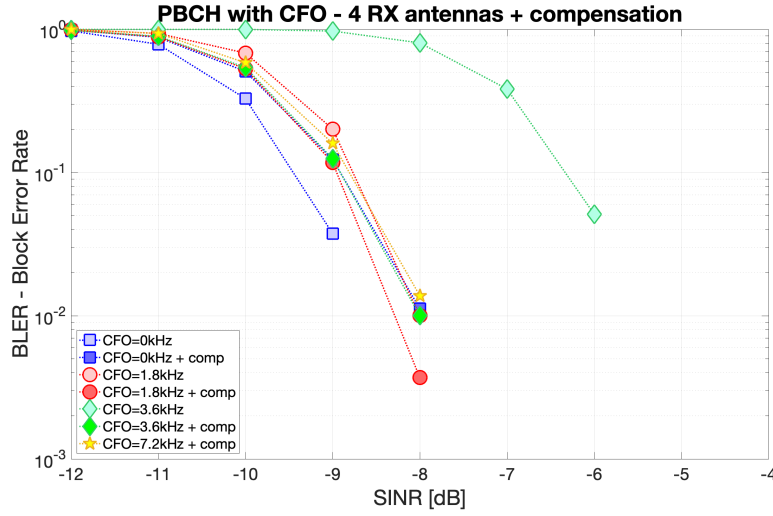


Figure 5.7: BLER for PBCH with CFO insertion and compensation, 4 RX antennas.

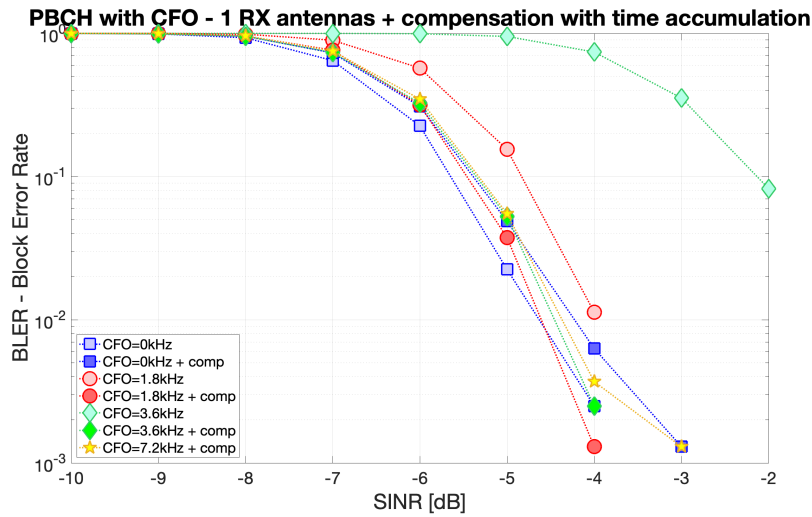


Figure 5.8: BLER for PBCH with CFO insertion and compensation with time accumulation, 1 RX antenna.

5.3 Timing analysis of the received signal

One of the PSS detection target is to recover the timing. Till now the radio channel module was not introducing any delay. In order to continuously add realistic parameters to the system, an extension of the simulator is then performed, simulating the time passed due to the propagation of the signal through the air.

To recover the interested delay the PSS detection is implied. After finding a peak in the correlation output, we can compute the affecting delay by looking at the difference

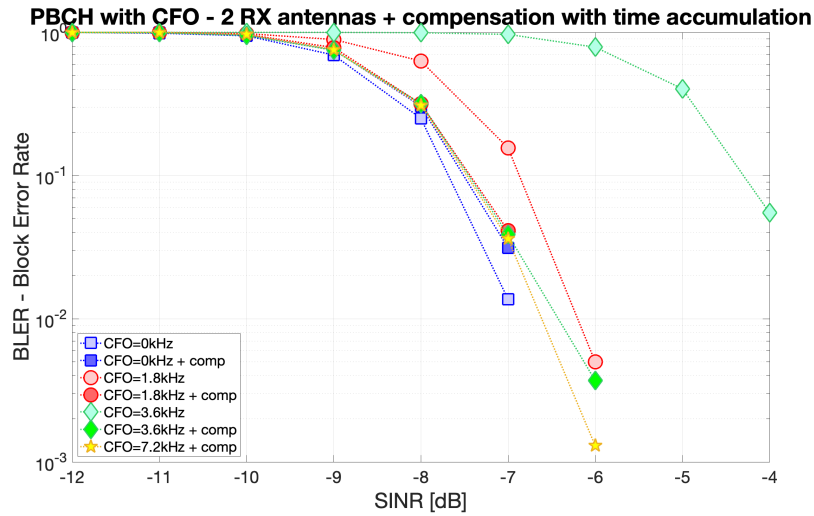


Figure 5.9: BLER for PBCH with CFO insertion and compensation with time accumulation, 2 RX antennas.

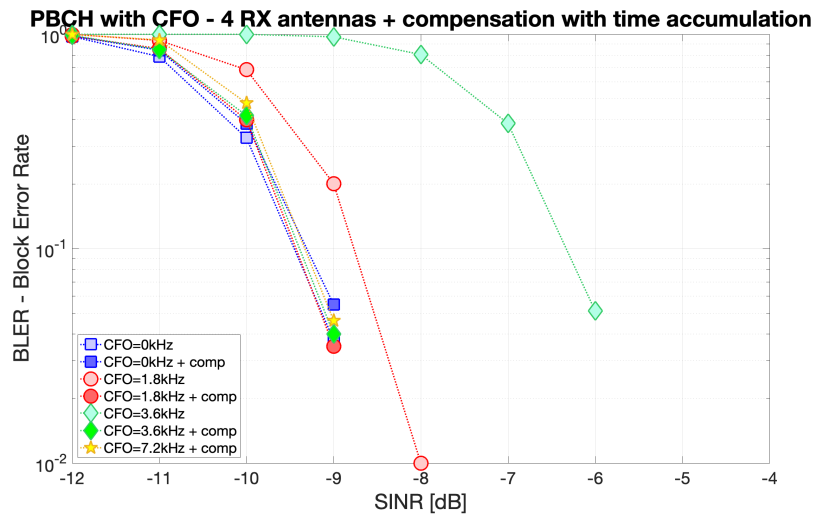


Figure 5.10: BLER for PBCH with CFO insertion and compensation with time accumulation, 4 RX antennas.

between the nominal position of the PSS in the slot, and the actual received one. The order of magnitude of the delay can be evaluated from the CP definition, since its length is computed w.r.t. the maximum delay spread. This means that we can choose almost any delay value smaller than the CP.

If the delay is not corrected, the transmission may be degraded. In particular in the OFDM demodulator, when the CP must be discarded, some of the samples of the CP would be instead maintained, while the same number of useful samples at the end

of the symbol would be lost. Fortunately, the CP is designed to avoid ISI, and the orthogonality is kept, but this sort of translation can still produce unpleasant effects. In order to simulate the propagation delay, we added a matched filter with coefficients corresponding to an array of all zeros except by one value, set to 1. The position of this last value corresponds to the desired delay. This step must save the samples that will exceed the maximum length of the slot, and restore them in the next step.

5.3.1 Propagation delay measurements

An interesting study can be done investigating how much the communication is hampered by the delay. Tests to analyse the scattering diagram and the errors in PBCH decoding have been performed in very high SINR scenario (100 dB), where noise can't affect the receiver behaviour. The impairments are then limited only on the delay. Two opposite cases can be identified:

1. Adding the delay: the signal propagates along the path and arrives at the receivers after a certain time, and nothing is applied to recover it. As shown in figure 5.11, RAW BER starts to appear at a delay comparable to the CP value, while BLER shows up with decoded BER when reaching a delay of almost two CPs. It increases quite rapidly, but it does not have a strictly threshold behaviour (not a vertical line). This seems to confirm that the CP helps to limit the delay effect till it's smaller than its length, even if the scattering diagrams still show a distortion of the modulation (figure 5.14a and figure 5.15a). Channel coding permits to recover the information also with delays exceeding the CP length, which delays introduce interference on subsequent OFDM symbols.
2. Overcompensation of the delay: the opposite situation than the previous one. It could represent a situation where the estimator is giving wrong delay estimates, bigger than the real one. We expect that this is a more critical situation than before, since sliding the FFT window in the opposite direction means falling into the successive OFDM symbol, without the protection of the CP, i.e. ISI shows up. In figure 5.12, the overall behaviour is similar to the first one, but, how we expected, degradation and distortion of the modulation comes up in advance (figure 5.14b and figure 5.15b).

In figure 5.13 the two BLER curves are compared. A basic expectation could be that the same BLER value for case 2 is present about CP number of samples before case 1 but, since the distortion is still affecting the signal inside the CP, this is not happening. In figure 5.16a and figure 5.16b the scattering diagram for values bigger than CP are shown. Huge degradations are clearly visible.

From this result we also derive that it could be useful to design a certain margin to apply on the delay estimates, in order to avoid overcompensation.

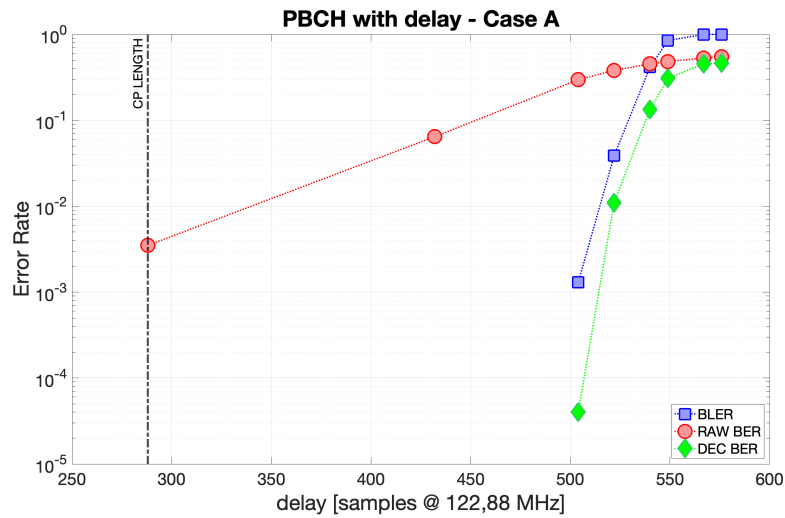


Figure 5.11: PBCH processing results w.r.t. delay, @ 100 dB SINR.

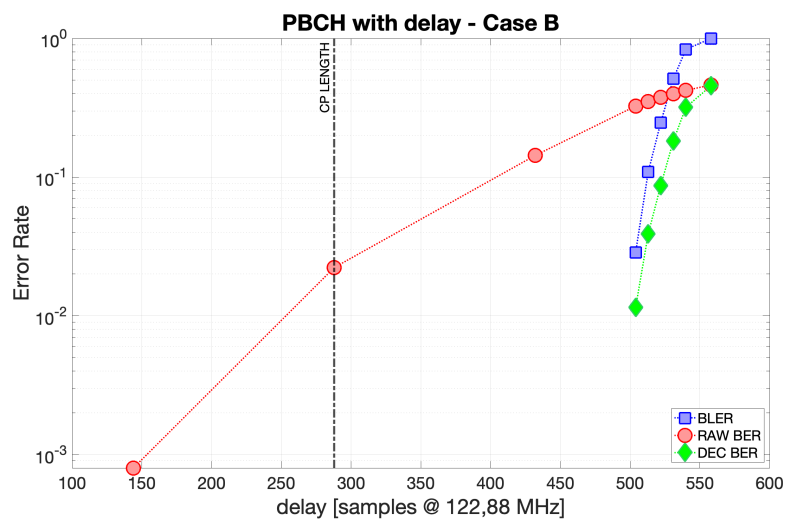


Figure 5.12: PBCH processing results w.r.t. delay overcompensation, @ 100 dB SINR.

5.4 Complete chain: PBCH processing with both CFO and delay

When moving to typical levels of SINR, the distortion caused by the delay combines with the noise degradation, leading to an increasing of errors in the PBCH processing even for delay values inside the CP length. For this reason we repeat the data collection done for the PBCH performance with CFO, inserting also the delayer.

Reasonable parameters chosen for this test are:

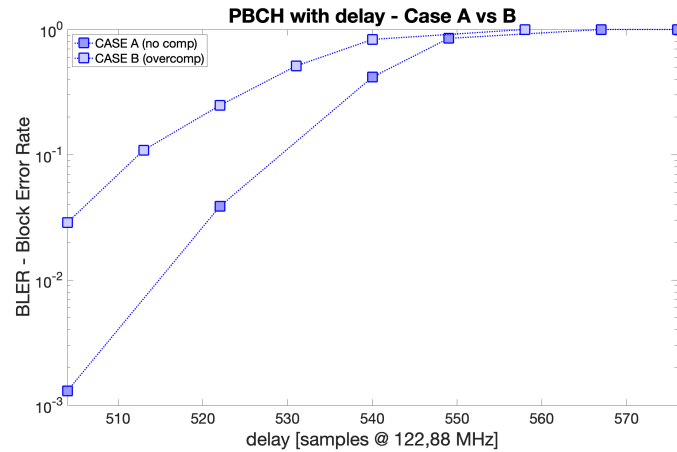
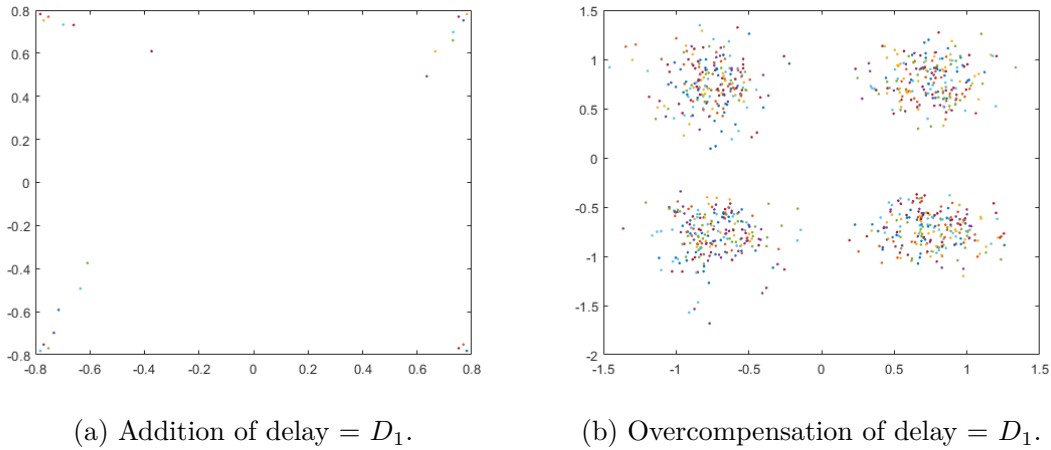


Figure 5.13: Comparison with the two timing cases, @ 100 dB SINR.



(a) Addition of delay = D_1 .

(b) Overcompensation of delay = D_1 .

Figure 5.14: Scattering diagrams @ 100 dB SINR, $D_1 = 144$ samples (1/2 CP)

- delay of 1/4 CP (72 samples @ 122.88 MHz)
- CFO of 1.8 kHz
- SIMO configuration 1x4 (4 RX antennas)
- Enabled time and space accumulation of CFO estimates

The output can be analysed in figure 5.17. Firstly, an ideal system is simulated, with neither CFO or delay. Then the two impairments are inserted in the transmission chain, with no counteracting. We can clearly see the bad effect on the BLER. If we apply the compensation provided by the PSS detection block, the BLER curve is much closer to the ideal case than the worst one (i.e., no compensation). In particular, there's at least 0.5 dB distance between the compensated and not compensated cases,

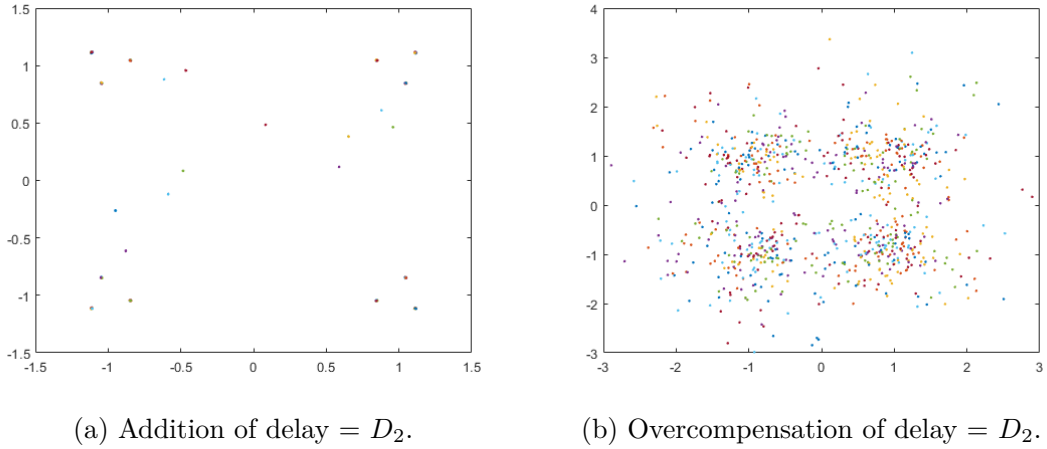


Figure 5.15: Scattering diagrams @ 100 dB SINR, $D_2 = 288$ samples (as CP length).

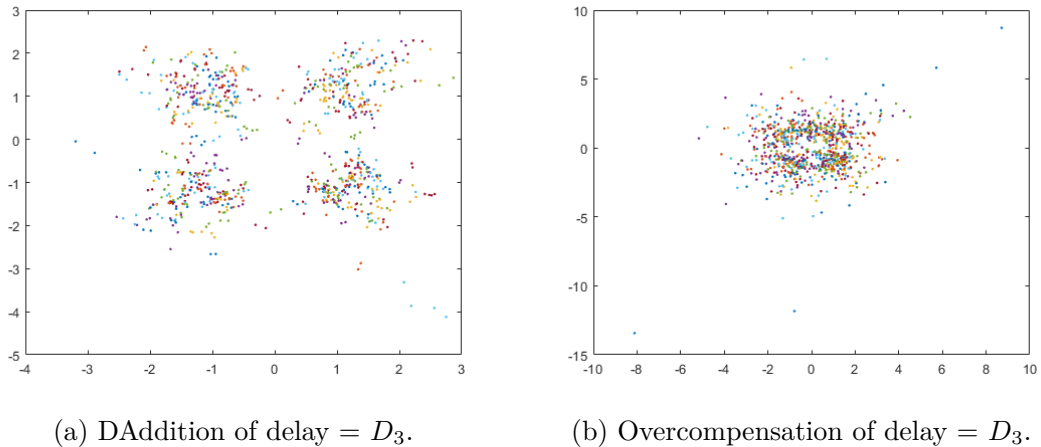


Figure 5.16: Scattering diagrams @ 100 dB SINR, $D_3 = 360$ samples (as CP length).

ad approximatively 0.1 dB from the ideal case to the compensated one. An increased complexity is of course the price of this result.

Given these evidences, we verified the good behaviour of the PSS synchronization step also in correcting the delay impairment.

Another test but with higher CFO (3.6 kHz) is reported in figure 5.18. Here the benefits from the compensation becomes much more evident.

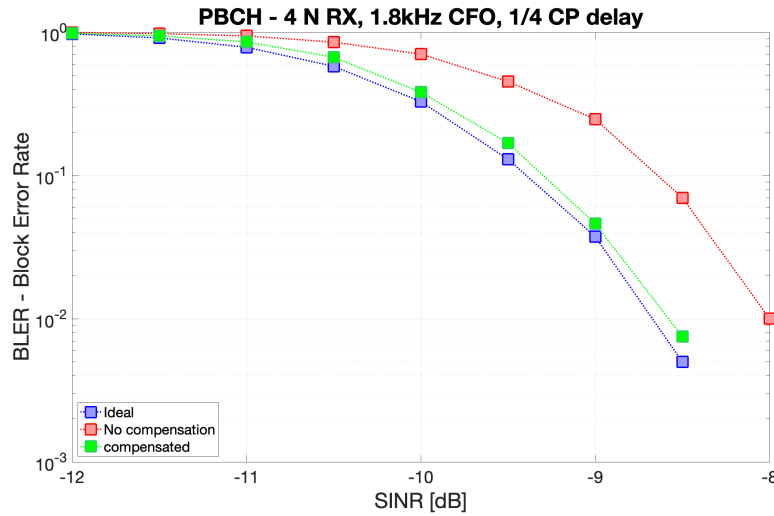


Figure 5.17: PBCH BLER behaviour with both delay and CFO (of 1.8 kHz) addition.

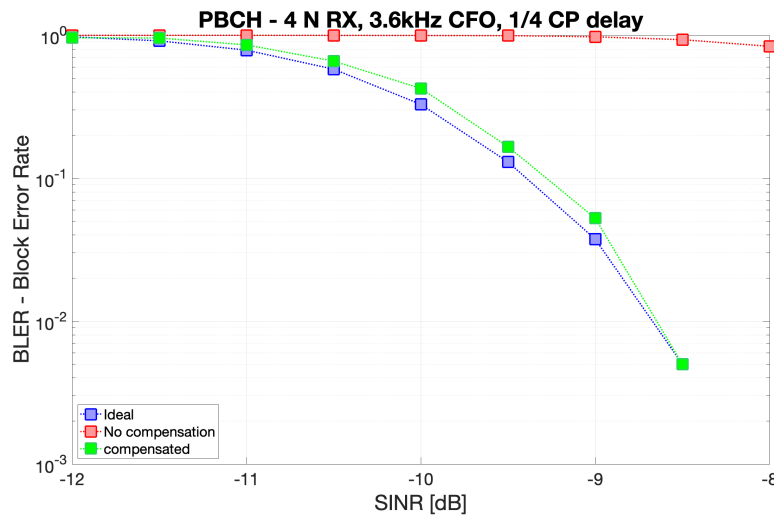


Figure 5.18: PBCH BLER behaviour with both delay and CFO (of 3.6 kHz) addition.

5.5 Simulations with fading channel and beamforming

In all the previous simulations the transmitter exploited only one antenna, so beamforming was not possible.

In this section instead we consider a 32x4 MIMO system, where the 32 antennas at the transmitter are used for beam-sweeping, with a set of beams covering the cell region taken from a codebook. By using some previous results, for each possible beam the gains measured at the receiver are obtained, and then the optimal beam directed

towards the receiver is identified. The tests we will now conduct are therefore taking into account the use of beamforming at the transmitter but, for reasons of computation duration, only the optimal beam will be employed, keeping it fixed for all the SSB transmissions², whose gain is about 10.4dB.

Moreover, a different type of channel model will be introduced, simulated through a 3GPP Clustered Delay Line (CDL) model with Non-line-of-sight (NLOS) propagation. This is for sure a more realistic condition, which tries to simulate the presence of several signal replicas (for example due to reflections and refractions generated by the environment) reaching the user from different directions and with different powers. We expect a significant drop in performance compared to the AWGN channel, since the multipath propagation of the channel causes destructive (or constructive) interference of the signal. In fact it is known also as fading channel, where the attenuation of the signal can change in a relatively rapid way, and does not depend only on the path loss. In figure 5.19 the BLER curves are reported. The ideal case is compared against the case with delay and CFO addition but no compensation, and with two different curves for the compensated case: the green one represents an averaging of CFO among 4 estimates, while the yellow one exploits up to 8 values. The longer averaging permits to keep the BLER closer to the ideal case, with an acceptable loss of 1 dB.

Looking at the RAW BER results in figure 5.20, we can see that the two compensation curves are actually overlapping. This can be explained by the fact that the compensation is working quite well, but, due to the greater impairments by the fading channel, sometimes a completely wrong CFO estimate can largely affect the compensation. It leads to errors in the polar decoder, impacting more the BLER than the RAW BER, since the latter is computed over a larger values of samples, while BLER depends on the entire decoded block correctness. Having a short time averaging the deviating values are only partly limited in their weight, and their effect keeps for some of the next compensations. By lengthening the set of offset estimates to be averaged, we can reduce the relevance of these spikes in the measurements, which we do not expect since the CFO should not vary too much in these temporal orders of magnitude. Other techniques could be considered, as a smarter averaging that sets smaller (or zero) weights to estimates that are too distant from the range of already obtained ones.

Delay measurements are usually quite reliable, so we do not expect errors in that case. However, at lower SINR values, the PSS detector suffers the fading channel more than the PBCH decoding, which can exploit channel estimation and compensation, or a polar decoding technique, pretty robust in this case. This increases the missed detection probability, and decreases its capability of estimation.

The presence of beamforming at the BS transmitter is not evident in these graphs, as the SINR values on the abscissa are those measured at the receiver, but we must remember that it is allowing us to obtain these results even if the channel SINR is about 10.4 dB lower without TX beamforming, so it is like the system is working in

²Each SSB within the SSB burst will still be considered independently, with the constraint of combining it, if necessary, only among the ones in the subsequent bursts

the case of a channel with SINR around -16 dB, not feasible for a real receiver to acquire synchronization with the BS.

We can remember that better results can then be obtained by enabling the soft combination of the PBCH by the receiver which, by combining 4 SSBs, can obtain a theoretical gain of 6 dB.

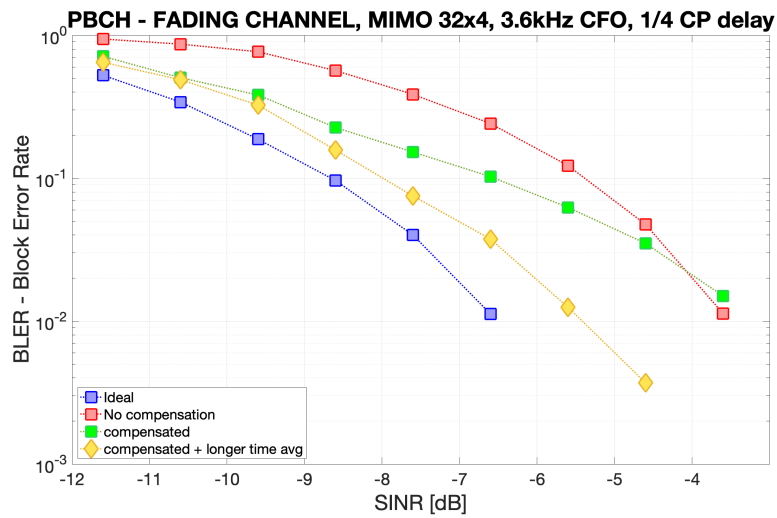


Figure 5.19: PBCH BLER behaviour for a 32x4 configuration with beamforming, fading channel and both delay (1/4 CP) and CFO (of 3.6 kHz) addition.

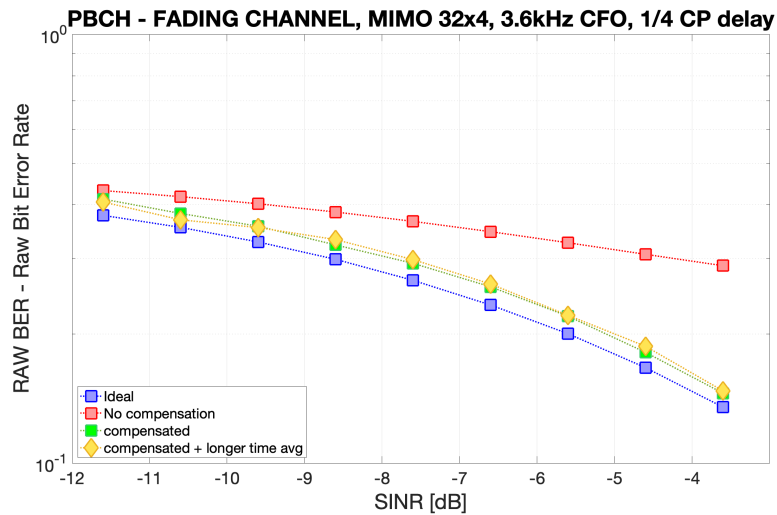


Figure 5.20: PBCH RAW BER behaviour for a 32x4 configuration with beamforming, fading channel and both delay (1/4 CP) and CFO (of 3.6 kHz) addition.

5.6 Extra considerations: a closed loop solution

We know that PSS detection is useful in many ways, and its CFO estimation can be considered as the acquisition stage (coarse estimation), that must be then followed by a tracking stage. This 2-step structure is a typical configuration of commercial systems. An example is reported in figure 5.21.

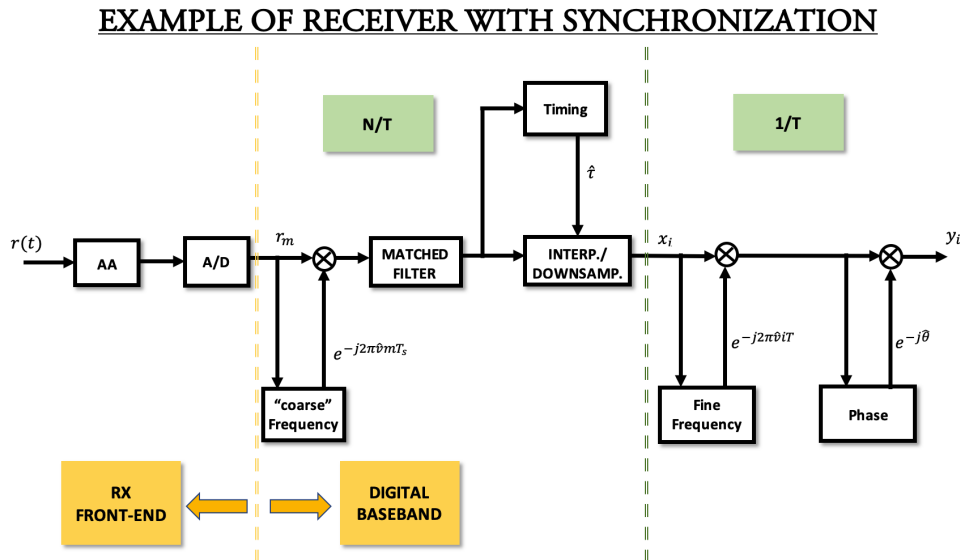


Figure 5.21: A block scheme example of RX with frequency acquisition and tracking.

The tracking stage is fundamental due to the Residual Carrier Frequency Offsets (RCFOs), generated by estimation errors and time-varying Doppler shifts, particularly relevant in high-mobility scenarios. RCFOs translates into linear phase shift, which must be compensated for.

Many techniques are available in the literature, some very sophisticated, and they can be classified as Data Aided (DA), Non-Data Aided (NDA) and blind methods. The most common and reliable solution is probably the DA method with pilot symbols³, which are widely used also for channel estimation. The NDA tracking method tries to preserve the spectral efficiency by exploiting the redundancy in the transmission scheme, as in the current communication standards employing OFDM, where there are signals presenting repetition features as primary synchronization signal (PSS), preamble, training sequence and cyclic prefix (CP). Blind approaches rely on the signal statistics and often have a very high computational complexity or extra requirements

³Symbols known both at transmitter and receiver side

on channel statistics. The tracking algorithms can be additionally aided by a prediction filter e.g. a Kalman filter.

Moreover, in OFDM systems a further division can be made in time or frequency domain operation. Acquisition instead is usually carried out in time domain, since at the initial stage the correct OFDM symbol disposal is not known (difficult to perform an accurate FFT by the OFDM demodulator)⁴.

This explanation is necessary to correctly place the CFO estimation technique discussed till now, which can be considered an acquisition stage in an open loop fashion (5.22a): there's no direct feedback after the PSS detection on the input signal, the correlation is always computed on the received signal without compensation, that is always performed after this step. The tracking stage must then be designed. It is not the main interest of our studies, also given that there are many different techniques and each UE provider can choose a different one. Anyway, a simple solution could be examined, by implementing a closed loop within the PSS detection step (as in figure 5.22b).

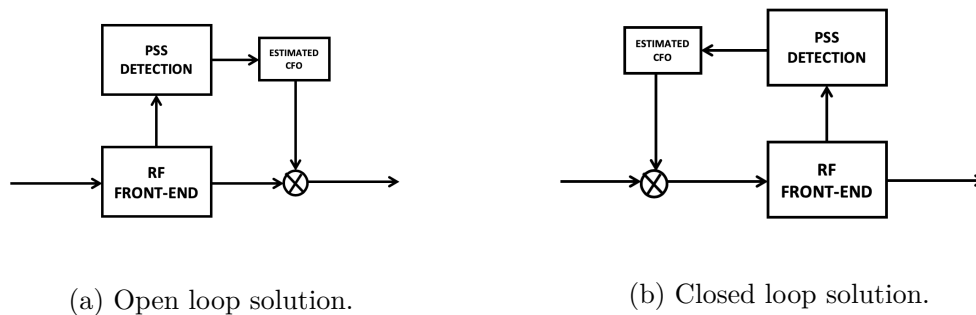


Figure 5.22: PSS detection module

We can already expect poor results from this type of implementation: we saw that the error of the CFO estimation can be pretty high and, without any sort of averaging, we doubt it will converge to the correct value. Some tests to check this hypothesis have been performed.

Working with the simulator allows us working firstly on a slot basis, repeating the estimate-compensate operations pair on the same slot for N times. From this solution an interesting results comes up: the magnitude of the estimates decreases at each iteration, and the CFO converges to a certain value. Unfortunately, this one can be pretty distant from the nominal CFO, with a distance that is comparable to the standard deviation magnitude. This means that the biggest problem of the estimator is not the precision, but the accuracy. Given a PSS sequence, it can measure a certain CFO with a relatively good precision, but this one is still probably a wrong one.

⁴Adapted from: [30], [31] and [32]

If we then try a more realistic scenario, applying instead the compensation on the next incoming slot, the system performs in a different way, but still badly: the error due to the inaccuracy propagates along the slots, decreasing the stability of the system.

Figure 5.23 shows the comparison between the CFO estimates distribution for open loop and closed loop implementation, respectively, for a nominal CFO of 3.6 kHz. Note that the first distribution is centred in 3.6 kHz while the second in 0 kHz, due to the compensation performed in the second solution.

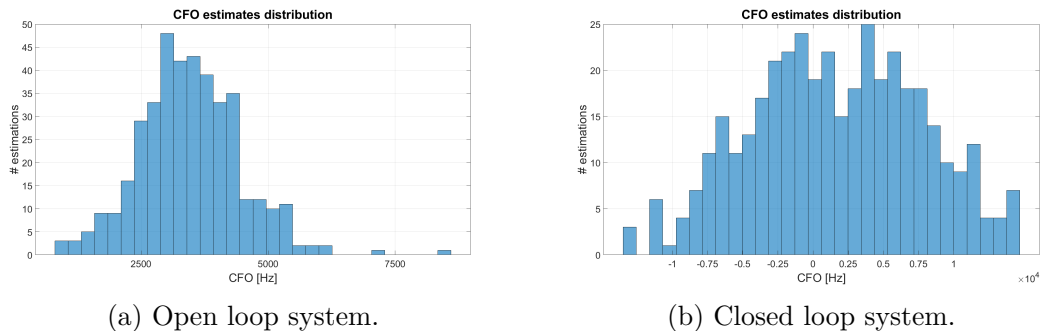


Figure 5.23: CFO estimates distribution.

We can assert that this closed loop solution with this CFO estimator is not suitable to improve the system performance or to be used as a sort of tracking stage. We should rely on the averaging techniques to improve the coarse CFO result and identify different techniques for the tracking stage. For example, in [34], it is presented the Phase Tracking Reference Signal (PT-RS) Design for 5G New Radio (NR), which aims to compensate from the mismatch of transmitter and receiver frequency oscillators, causing the so-called phase noise.

Chapter 6

Conclusions

Synchronization plays a fundamental role in 5G, in order to speed up network access procedures and therefore reduce initial latencies, to comply with even more stringent alignment requirements over time (as for TDD systems), to take advantage of new techniques such as beamsweeping, essential in view of the new high frequency bands, and more. The numerous tests carried out show how the transition from technical specifications to actual implementations requires careful analysis, considering the variety of situations and hardware devices availability, which can lead to stringent limits on the study.

The PSS detection shows the good correlation properties of the m-sequences, so within reasonable limits of SINR and CFO the system performs well. Particular attention is required in the design of the Anti Aliasing (AA) filter, to avoid the onset of ISI which would put a strain on the detector. In addition, a correct definition of the threshold is also necessary to limit false positives, to be avoided as much as possible. In case of fading channel, however, there may be some time instants in which the reception quality is so low as to prevent peak detection. Unlike PBCH in fact, the PSS cannot be subjected to data transformations such as interleaving, which would increase the robustness of reception in the event of burst errors.

Regarding the CFO of the signal, a frequency offset estimator can be obtained from the detector, but it seems to suffer from a not negligible variance, also given by the limit on the length of the matched filter for correlation. To make the CFO estimate more precise, a simple averaging over time lead to clear improvements, but even more sophisticated techniques could be considered, provided that low complexity is respected. The estimation of the delay is of course essential to correctly locate the arrangement of the OFDM symbols in the time domain, and therefore apply the demodulation. Time synchronization will be even more important than in the past, since 5G makes extensive use of Time Division Duplexing (TDD). The detector turns out to be very precise in this task, except for the few cases of missed detection and false alarm which are however physiologic for threshold detectors.

Interesting is the simulation of a transmitter performing beam-sweeping, which allows to increase the gain in the direction of the receiver but which could also increase the

duration of the cell search.

After the PSS detection phase it has been studied the influence of the previous processes on the PBCH, strongly dependent on the cell identifier obtainable from PSS and SSS. MIMO systems show their usefulness here, whereby increasing the number of antennas at the receiver allows for improved performance (measured in terms of BLER) as we could have expected. The simulator therefore made it possible to verify the transmission chain in a very varied set of configurations and parameters, providing useful results from the 5G implementation point of view. PBCH decoding can be deteriorated a lot by the CFO, so its accurate estimation and compensation is required. The SSS study has not been thoroughly analysed, but further studies may investigate its behaviour and possible use to refine the measurement of the CFO.

Considering the ultra-dense architecture of the new standard, it will be important to further study the behaviour of the receiver when different transmissions overlap in the radio channel, distinguishing the various cells that interfere with each other. This can be done for example with a System Level simulators, which still need the results from a Link Level Simulator to have a complete view of the network.

Subsequently the studied algorithms will be implemented in hardware through FPGA systems, possibly adapted to a fixed point rather than floating point notation.

Bibliography

- [1] E. Dahlman, S. Parkvall, J. Skold, "What Is 5G?". In: *5G NR: The Next Generation Wireless Access Technology*, Elsevier, Ch. 1, pp. 1-6, 2018
- [2] J. Rodriguez, *Fundamentals of 5G mobile networks*. Chichester: Wiley, Ch.1, pp. 1-25, 2015
- [3] 3GPP, *3gpp TSG SA # 87e*, 17-20 March 2020, <https://www.3gpp.org/release-16>
- [4] Huawei Technologies Co., *5G Network Architecture - A High-Level Perspective*, 2016, https://www.huawei.com/minisite/5g/img/5G_Network_Architecture_A_High-Level_Perspective_en.pdf
- [5] 3GPP, *5G; Service requirements for next generation new services and markets*, ETSI TS 22.261 version V15.5.0 (Release 15), July 2018
- [6] *Cisco Visual Networking Index : Global Mobile Data Traffic Forecast Update, 2015-2020*, Cisco, White Pap., pp. 1–39, February 2016
- [7] C. Bockelmann, N. K. Pratas, G. Wunder, S. Saur, M. Navarro, D. Gregoratti, . . . A. Dekorsy, (2018). *Towards Massive Connectivity Support for Scalable mMTC Communications in 5G Networks*, IEEE Access, 6, 28969-28992. doi:10.1109/access.2018.2837382
- [8] S. K. Rao, R. Prasad, *Impact of 5G Technologies on Industry 4.0*, Springer, 13 March 2018
- [9] E. Dahlman, S. Parkvall, J. Skold, "Spectrum for 5G". In: *5G NR: The Next Generation Wireless Access Technology*, Elsevier, Ch. 3, pp. 27-37, 2018
- [10] R. Haupt, *Antenna arrays*, Hoboken, N.J.: Wiley-IEEE Press, 2010.
- [11] E. Dahlman, S. Parkvall, J. Skold, "NR Overview". In: *5G NR: The Next Generation Wireless Access Technology*, Elsevier, Ch. 5, pp. 1-6, 2018
- [12] Ericsson, *New Ericsson software makes the shift to Standalone 5G easier*, <https://www.ericsson.com/en/press-releases/2020/7/new-ericsson-software-makes-the-shift-to-standalone-5g-easier>, Press Release, 6th July 2020
- [13] S. Lambert, W. V. Heddeghem, W. Vereecken, B. Lannoo, D. Colle, M. Pickavet, *Worldwide electricity consumption of communication networks*, Optics Express, 20(26), December 2012, doi:10.1364/oe.20.00b513
- [14] G. Buttazoni, F. Babich, R. Tuninato, F. Vatta, and M. Comisso, *Phase-only pattern synthesis with interference suppression for large-scale antenna arrays*, in Int. Conf. Appl. Electromagn. Commun. (ICECOM), Dubrovnik, Croatia, pp. 1 - 6, 30 Sept.-2 Oct. 2019

-
- [15] A. Galis, J. Dong, K. Makhijani, S. Bryant, M. Boucadair, P. Martinez-Julia, *Network Slicing - Introductory Document and Revised Problem Statement*, Internet-Draft draft-gdmb-netslices-intro-and-ps-02, February 2017
- [16] M. Zarri, K. Qin, *Network Slicing - Use Case Requirements*, GSMA Future Networks Programme, April 2018
- [17] G. Ancans, A. Stafecka, V. Bobrovs, A. Ancans, J. Caiko, *Analysis of Characteristics and Requirements for 5G Mobile Communication Systems*, Latvian Journal of Physics and Technical Sciences, 54(4), pp. 69-78, 2017, doi:10.1515/lpts-2017-0028
- [18] J. Lin, *Synchronization Requirements for 5G: An Overview of Standards or Specifications for Cellular Networks*, IEEE Vehicular Technology Magazine, 13(3), 91-99, June 2018, doi: 10.1109/mvt.2018.2813339
- [19] A. Omri, M. Shaqfeh, A. Ali, H. Alnuweiri, *Synchronization Procedure in 5G NR Systems*, IEEE Access, 7, 41286-41295, April 2019, doi: 10.1109/access.2019.2907970
- [20] E. Dahlman, S. Parkvall, J. Skold, "Initial Access". In: *5G NR: The Next Generation Wireless Access Technology*, Elsevier, Ch. 16, pp. 311-334, 2018
- [21] D. Chandramouli, R. Liebhart, J. Pirskanen, "Radio Access Technology". In *5G for the Connected World*, Hoboken, NJ: Wiley, Ch. 3, pp. 51-125, 2019
- [22] 3GPP, *5G; NR; Physical channels and modulation*, ETSI TS 138 211 V15.2.0 (Release 15), July 2018
- [23] Y. Kryukov, D. Pokamestov, E. Rogozhnikov, *Cell search and synchronization in 5G NR*, ITM Web of Conferences 30 04007, 2019, doi:10.1051/itmconf/20193004007
- [24] 3GPP R1-1715093, *NR PBCH Design*, Intel Corporation, 3GPP TSG-RAN WG1 Meeting #90, Prague, Czech Republic, August 21th – 25th, 2017
- [25] 3GPP R1-1713375, *PBCH and PBCH DMRS design consideration* Qualcomm, 3GPP TSG-RAN WG1 Meeting #90, Prague, Czech Republic, August 21th – 25th, 2017
- [26] K. Niu, K. Chen, J. Lin, Q. T. Zhang, *Polar Codes: Primary Concepts and Practical Decoding Algorithms*, IEEE Communications Magazine, 52(7), 192-203, July 2014, doi:10.1109/mcom.2014.6852102
- [27] 3GPP, *LTE; 5G; Study on channel model for frequency spectrum above 6 GHz*, ETSI TR 138 900 14.2.0 (Release 14), June 2017
- [28] K. Ota, M. Sawashi, A. Shimura, S. Nagata, *Performance of Physical Cell ID Detection Probability Considering Frequency Offset for NR Radio Interface*, IEEE 90th Vehicular Technology Conference (VTC2019-Fall), November 2019
- [29] ETSI TS 138 101-1 V15.2.0, *Technical specification: 5G; NR; User Equipment (UE) radio transmission and reception; Part 1: Range 1 Standalone*, 3gpp, July 2018
- [30] P. Sun, M. Morelli, L. Zhang, *Carrier Frequency Offset Tracking in the IEEE 802.16e OFDMA Uplink*, IEEE TRANSACTIONS ON WIRELESS COMMUNICATIONS, VOL. 9, NO. 12, December 2010
- [31] L. Koschel, A. Kortke, *Frequency Synchronization and Phase Offset Tracking in a Real-Time 60-GHz CS-OFDM MIMO System*, IEEE 23rd International Symposium on Personal, Indoor and Mobile Radio Communications, 2012

- [32] J. Kim, J. Moon, S. Bahng, Y. Bang, Y. Park, *A Research on Carrier Frequency Offset Estimation for 5G Telecommunication*, Electronics Telecommunications Research Institute, Giga Transmission Research Team Daejeon, Republic of Korea, 2014
- [33] 3GPP, *5G; Study on New Radio (NR) access technology*, ETSI TR 138 912 V14.0.0 (Release 14), May 2017
- [34] Q. Yinan, M. Hunukumbure, H. Nam, H. Yoo, and S. Amuru, *On the Phase Tracking Reference Signal (PT-RS) Design for 5G New Radio (NR)*, Samsung Electronics R and D Institute UK, 2018
- [35] C. Beccari, *Il pacchetto TOPtesi*, 6.4.06, September 2020, <http://mirrors.ibiblio.org/CTAN/macros/latex/contrib/toptesi/toptesi-it.pdf>